*School of Molecular and Cell Biology*

*University of the Witwatersrand*

*Johannesburg*

# Investigating Telomere Dynamics in Oesophageal Squamous Carcinoma Cells using Standard and Gold Nanoparticle-based Assays

---

Martin Bernert

Student No. 375076

A Dissertation submitted to the Faculty of Science, University of the Witwatersrand, in fulfilment of the requirements for the degree of Master of Science

Johannesburg, 2017

**Table of Contents**

**Declaration**

I, Martin Bernert (375076), am a student registered for the degree of Masters of Science (MSc) in the academic year 2015-2016.

I hereby declare the following:

- I am aware that plagiarism (the use of someone else's work without their permission and/or without acknowledging the original source) is wrong.
- I confirm that the work submitted for assessment for the above degree is my own unaided work except where explicitly indicated otherwise.
- I have not submitted this work before for any other degree or examination at any other University.
- I have followed the required conventions in referencing the thoughts and ideas of others.
- I understand that the University of the Witwatersrand may take disciplinary action against me if there is a belief that this is not my own unaided work or that I have failed to acknowledge the source of the ideas or words in my writing.

Signature:  Date: 23.06.2017

## List of Abbreviations

| Abbreviation | Meaning |
|---|---|
| A, C, G, T | Adenine, Cytosine, Guanine, Thymine |
| ALT | Alternate Lengthening of Telomeres |
| AMPK | Adenosine Monophosphate Activated Protein Kinase |
| AuNPs | Gold Nanoparticles |
| bp | Base Pairs |
| c-DNA | Complimentary DNA |
| CHAPS | 3-[(3-Cholamidopropyl)dimethylammonio]-1-propanesulfonate |
| DIG | Digoxigenin |
| DMEM | Dulbecco's Modified Eagle's Medium |
| DMSO | Dimethyl sulfoxide |
| DNA | Deoxyribonucleic acid |
| DNase | Deoxyribonuclease |
| dNTP | Deoxyribonucleotide |
| EDTA | Ethylene diaminetetraacetic acid |
| ELISA | Enzyme-linked Immunosorbent Assay |
| GAPDH | Glyceraldehyde-3-phosphate Dehydrogenase |
| hTERC | Human Telomerase RNA Component |
| hTERT | Human Telomerase Reverse Transcriptase |
| ILK | Integrin-linked Kinase |
| LKB1 | Liver Kinase B1 |
| mRNA | Messenger Ribonucleic Acid |
| MTT | 3-(4,5-dimethylthiazol-2-yl)-2,5-diphenyltetrazolium bromide |
| PBS | Phosphate Buffered Saline |
| PCR | Polymerase Chain Reaction |
| POT1 | Protection of Telomere 1 |
| QDs | Quantum Dots |
| qPCR | Quantitative Polymerase Chain Reaction |
| RAP1 | Repressor/Activator Protein 1 |
| RNA | Ribonucleic acid |
| RNase | Ribonuclease |
| ROS | Reactive Oxygen Species |
| SNP | Single Nucleotide Polymorphism |
| SP1 | Specificity Protein 1 |
| TRAP | Telomeric Repeat Amplification Protocol |
| SEM | Scanning Electron Microscopy |
| STELA | Single Telomere Length Analysis |
| TEM | Transmission Electron Microscopy |
| TIN2 | TRF1 Interacting Nuclear factor 2 |
| TPP1 | TINT1, PTOP, PIP1 — POT1-TIN2 organizing protein |
| TRF1/2 | Telomeric repeat-binding factor 1/2 |
| UV | Ultraviolet |
| VNTR | Variable Number of Tandem Repeats |

## List of Figures

**List of Tables**

**Conference Outputs:**

M. Bernert, T. C. Otgaar, P. Baichan, S.T. Malindisa, S.F.T Weiss, R. B. Veale, S. Moeno and B.T. Letsolo. Investigating Telomere Dynamics in Oesophageal Squamous Carcinoma Cells using Standard and Nanoparticle-based Assays. Molecular Biosciences Research Thrust (MBRT) Research Day. 08.12.2016. (Poster Presentation).

**Acknowledgements**

I would like to thank my supervisor Dr. Boitelo T. Letsolo for her constant support and guidance throughout my honours and masters as well as for the opportunity to learn a multitude of interesting and challenging techniques.

I would also like to thank my new supervisor Prof. Stefan F.T. Weiss for all his help and for motivating me to do my best. I would like to especially thank him for taking me on as his student after Dr. Letsolo tragically passed away and his lab for making me feel welcome and part of the team as well as my advisor Dr. Kulsum Kondiah for all her support.

I would also like to thank my great friends and lab partners Sibusiso Malindisa, Tyrone Otgaar and Pavan Baichan for their patience, help and advice throughout my studies, without them the years would never have been as enjoyable.

I would like to thank Dr. Sharon Moeno, for the use of her lab as well as her invaluable guidance concerning nano-chemistry, as well as her student Maxwell Thatyana for his advice on nanoparticle synthesis.

Prof. Robin B. Veale deserves my gratitude for allowing me to use his oesophageal cancer cell lines.

I would also like to thank my parents for their love and support throughout the master's program.

Finally, I would like to thank University of the Witwatersrand Faculty of Science for funding this project as well as the Postgraduate Merit Award (PGMA) and National Research Foundation (NRF) for funding.

**Abstract**

Cancer is characterised by abnormal cell proliferation and is one of the leading causes of death in first world countries and the second leading cause in developing countries. In 2012 alone, over 14 million cases were reported and over 8 million deaths were attributed to cancer worldwide, with sub-Saharan Africa, especially South Africa having one of the highest oesophageal cancer rates in the world. An important aspect of cancer is the telomeres, which are 10-15kbp of TTAGGG DNA repeats in humans at the ends of chromosomes. These repeats are maintained by the enzyme telomerase. Up to 90% of all cancers show increased telomerase activity to overcome the "end-replication" problem in which the telomeres shorten after each cell division. This eventually leads to cellular senescence. Due to the high number of cancers relying on increased telomerase activity to bypass senescence, telomerase could be a viable target for anti-cancer therapies. The limiting factor of the multi-subunit telomerase enzyme is its telomerase reverse transcriptase component (hTERT). hTERT has also been shown to migrate to the mitochondria during times of high oxidative stress caused by reactive oxygen species (ROS). Here it confers protection to the mitochondria against ROS, potentially preventing the cell form undergoing apoptosis and reaching senescence. This can potentially be detrimental, as cells become damaged by the ROS and continue dividing. This could lead to further genetic damage. Metformin, a drug used for the treatment of type-2 diabetes, has been linked to lower incidences of cancer. The mode of action of metformin is not yet fully understood, however it is known that it affects the mitochondria. Since hTERT and metformin could co-localise, the drug may influence hTERT and potentially telomerase activity. This makes metformin an anticancer candidate to be used in conjunction with traditional anticancer therapies.

To determine telomerase activity in metformin treated oesophageal carcinoma cells, qPCR based telomerase activity assays must be used. These assays can be very expensive and time consuming, so a faster and cheaper alternative would be beneficial. Therefore, the aim of this project was to alter and improve a nanoparticle based detection method for telomerase activity, by decreasing the time required to

prepare the DNA functionalised nanoparticles as well as determining a more rapid method of data measurement, and compare it to conventional qPCR based techniques (TRAPeze RT Telomerase Activity Kit – Merck). Thereafter the effects of the metformin treatment on telomere dynamics, such as telomere length, telomerase activity and hTERT mRNA expression, in oesophageal squamous carcinoma cells were determined.

Gold nanoparticles were synthesised and functionalised with thiolated-DNA (telomerase substrate). These functionalised particles were characterised using transmission electron microscopy. To assess telomerase activity the extracted protein was added to the functionalised nanoparticle solution and allowed to elongate the coupled DNA. A characteristic of gold nanoparticles is that the size of the particles as well as their proximity to one another determines the colour of the nanoparticle solution. Due to the steric hindrance caused by the now elongated DNA, a distinct colour change was observable. The change in absorption spectra of the nanoparticle solution was recorded after the enzyme elongated the substrate. This nanoparticle based assay was then compared to TRAPeze RT Telomerase detection kit (Merck-Millipore) as a positive control. Using the conventional qPCR based telomerase activity assay, it was found that metformin significantly decreased telomerase activity in oesophageal cancer cell lines, however this was not seen using the nanoparticle assay. A colour change was observed with the nanoparticle assay compared to the negative control reflecting detection of telomerase activity. However, no significant decrease in telomerase activity could be detected due to metformin treatment.

More optimisation is required, however this technique has great potential, as nanoparticle based assays are also known for their high sensitivity. This technique is also far more rapid and significantly cheaper that the qPCR based method. The gold nanoparticle based telomerase activity assay could become an alternative to conventional qPCR based techniques.

## 1 Introduction and Literature Review:

Using molecular biology and genetics techniques, telomere dynamics were assessed in metformin treated oesophageal squamous cell carcinoma cell lines. This included telomerase activity, human telomerase reverse transcriptase (hTERT) mRNA expression and telomere length. In addition, a modified telomerase activity assay, utilizing gold nanoparticles (AuNPs), was developed in order to find an alternative to conventional qPCR based methods. DNA-functionalised AuNPs were produced and the assay compared to the standard qPCR based telomeric repeat amplification protocol (TRAP). The different aspects of this project are discussed below.

### 1.1 Oesophageal Cancer:

Cancer is characterised by abnormal cell proliferation and is one of the leading causes of death in first world countries and the second leading cause in developing countries (Jemal et al., 2011). In 2012 alone, over 14 million cases were reported and over 8 million deaths were attributed to cancer worldwide, whereas in sub-Saharan Africa over 14,000 cases were reported (Ferlay et al., 2012). Oesophageal cancer proved to be the 8$^{th}$ most common cancer, causing over 400,000 deaths estimated in 2012 (Ferlay et al., 2012). It has been found that southern Africa has an extremely high incidence rate, with South Africa in particular having the highest incidence rate in the world (Arnold et al., 2015). Oesophageal carcinoma is the 4$^{th}$ most diagnosed cancer for men and the 5$^{th}$ most prevalent cancer for woman in South Africa (GLOBOCAN 2012). There are two main types of oesophageal cancer and both have slightly different causes and are more prevalent in different parts of the world. The first, oesophageal adenocarcinoma, which generally presents itself within the lower third of the oesophagus, is more common in first world countries. On the other hand, oesophageal squamous cell carcinoma is more common in developing countries and presents itself in the upper two thirds of the oesophagus. There are many different risk factors for oesophageal cancer, the most common of which include: cigarette smoking, environmental pollutants, as well as excess alcohol consumption (Brown et al., 2001; Domper Arnal et al., 2015).

Due to the risk of metastasis in late stage oesophageal cancer, it can be difficult to treat if not detected early. Like for many cancers, there are three main treatment options available, each of which presents its own set of risks. Surgery, chemotherapy and radiation therapy can come with severe side effects, which can include diarrhoea, nausea, non-specific destruction of healthy cells as well as the suppression of one's immune system (Lawenda et al., 2008). Due to these side effects in addition to the ineffectiveness of the treatment options at late stage oesophageal cancer, the importance of finding alternative therapies cannot be overstated.

## 1.2 Telomeres:

### 1.2.1 Structure:

Telomeres consist of 10-15kbp of double stranded TTAGGG DNA repeats in humans and are found at the ends of chromosomes (reviewed in Fleming and Burrows, 2013). Telomeres have a 3′ overhang which is used to form secondary structures. To form structures such as the telomere loop (t-loop) (Figure 1.1), the 3′ overhang is folded back on itself. These structures in conjunction with other telomere stabilising proteins, including the telosome, a multi-protein structure also known as the "shelterin" complex (Figure 1.2), help stabilise the ends of chromosomes. The t-loop and the shelterin complex prevent chromosome degradation and fusion, in doing so regulating telomere length (Bailey and Murnane, 2006).

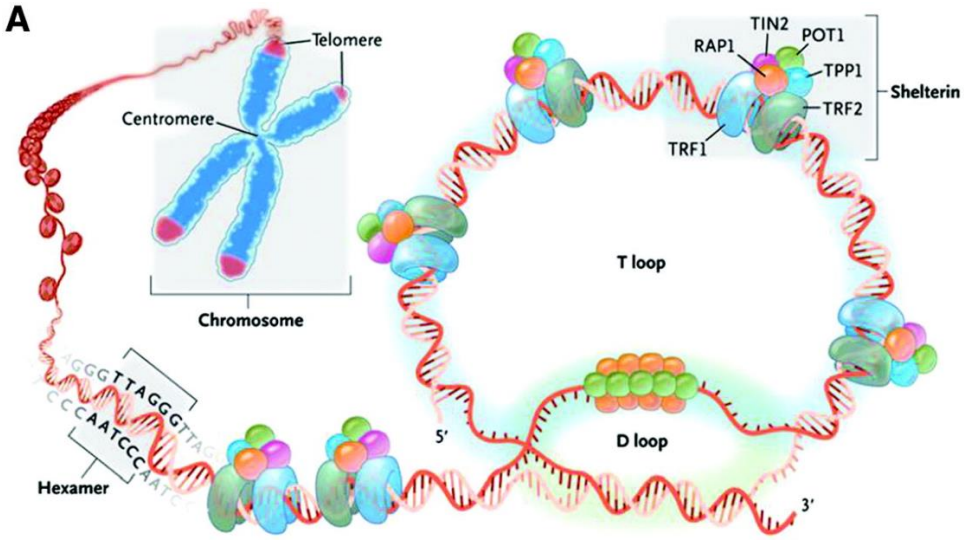


Figure 1.1: Diagram of the Telomere Loop (t-loop). This image shows the t-loop fold, as well as associated binding proteins. The red strand of DNA shows the 3' overhang, which folds over to form the t-loop. TRF1 (blue disc) and TRF2 (dark green disc) are shown in conjunction with the rest of the shelterin complex to be stabilising the t-loop (adapted from Kovacic et al., 2011).

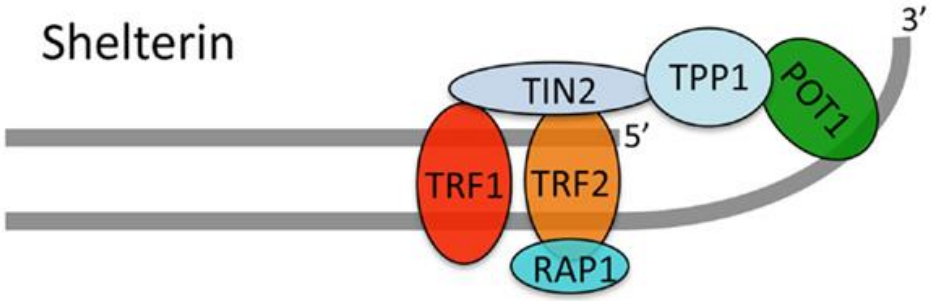


Figure 1.2: Graphical Representation of the "Shelterin" Complex (Raffa et al., 2013). This protein complex consists of six main proteins: RAP1, TRF1, TRF2, TIN2, POT1 and TPP1. Of these proteins, POT1 binds directly to single stranded telomeric DNA whereas TRF1 and 2 bind to double stranded telomeric DNA. The other components of the complex however, help stabilise and link the protein complex together (Bailey and Murnane, 2006).

1.2.2 Function:

As previously mentioned, telomeres help stabilise the far ends of chromosomes. They carry out this protective function by preventing the erosion of important coding DNA by the “end-replication” problem (Levy et al., 1992). This loss of coding DNA occurs because of the incomplete synthesis of double stranded DNA, which is a characteristic of the mode of action of RNA dependant DNA polymerase (Figure 1.3). The polymerase utilises an RNA primer in order to synthesise a new DNA strand. A single stranded overhang remains after synthesis however, due to the subsequent degradation of the RNA primer (Levy et al., 1992). This overhang is then removed, which results in the loss of small fragments of DNA after each synthesis reaction (reviewed in Denchi, 2009). Therefore this leads to the systematic erosion of the ends of chromosomes after cell division (Blackburn, 1991).

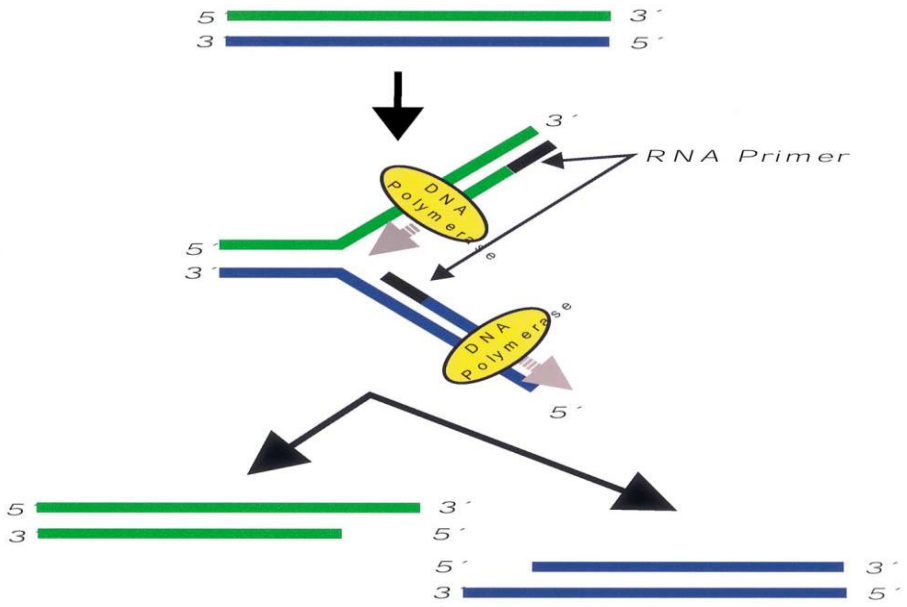


Figure 1.3: Schematic Representation of the "End-Replication" Problem (Klapper et al., 2001). This diagram represents the DNA synthesis reaction, performed by DNA polymerase. Both the leading strand (green) and the lagging strand (blue) of the replication fork are shown with an attached RNA primer. As this RNA primer is degraded, the newly

synthesised double stranded DNA is missing complimentary bases on the 5′end, leading to a 3′ overhangs in the template strand.

Telomeres act as a "buffer" zone to this erosion. If, however they are not continually maintained after each cell division, it will lead to the degradation of coding DNA. The enzyme telomerase, which is a multi-subunit protein, maintains the telomeres. Telomerase has been shown to be nearly undetectable in most somatic cell lines (Kim et al., 1994). Germ-line cells in addition to other highly proliferating cell types, such as intestinal and oesophageal cells, have been shown to have high telomerase activity. This is most likely due to these cell types requiring to undergo constant cell division (Kim et al., 1994; Wright et al., 1996). If the telomeres are not maintained and a functional DNA damage repair mechanism, such as p53, is still intact, it could lead to replicative senescence (where cells are metabolically active, but no longer replicate) or even the induction of apoptosis (programmed cell death) (reviewed in Shay and Wright, 2005). Taking this into consideration, DNA damage response pathways and telomere dynamics can play a vital role in the progression of diseases such as cancer, due to its characteristic uncontrolled cell proliferation (Figure 1.4). Normally, somatic cells are only capable of undergoing a limited number of cell divisions because of the shortening of telomeres. This is known as the "Hayflick limit" (Hayflick and Moorhead, 1961). When approaching this limit, it can lead to the disruption of normal tissue function, which has been theorised to contribute to the aging process (Sahin and Depinho, 2010; Carneiro et al., 2016). This is further supported by the fact that older individuals have shorter telomeres (Harris et al., 2012). This has led to the telomere theory of ageing.

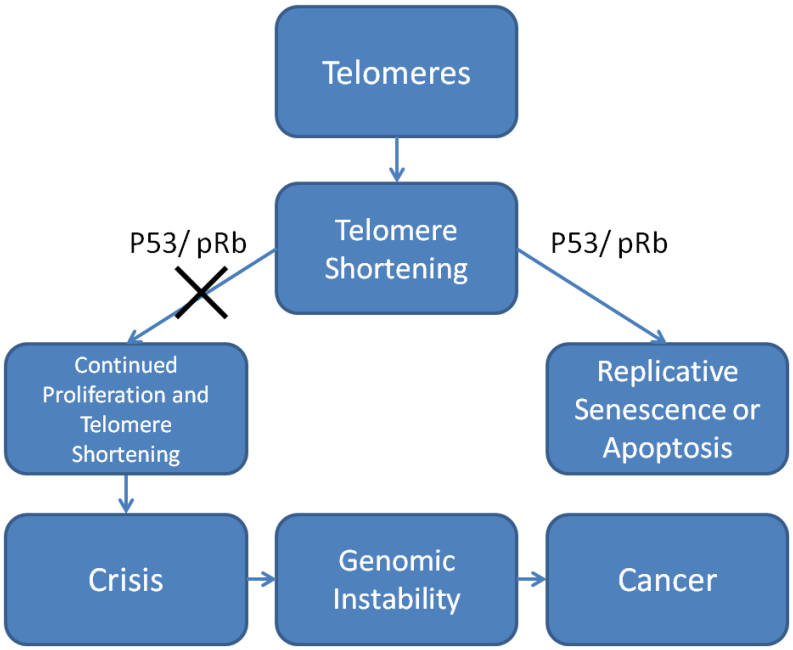


Figure 1.4: Flow Diagram of Cellular Crisis. This diagram shows the relationship of telomere shortening in the presence and absence of functional DNA damage repair mechanisms (Retinoblastoma protein (pRb) and p53). In the presence of functional mechanisms, the cell will undergo apoptosis or replicative senescence, whereas without these mechanisms, telomere shortening can progress to cellular crisis. This can subsequently lead to genomic instability and even cancer.

### 1.2.3 Telomeres and Cancer:

As previously mentioned, telomeres are vital for continued cell proliferation, and therefore have an important role in cancer genetics. Since continued cell division leads to telomere shortening, DNA damage repair pathways such as the p53 pathway can be triggered, causing cell cycle arrest (senescence) and even apoptosis (Shay and Wright, 2005). Consequently, senescence acts as a tumour suppressor mechanism, which needs to be circumvented by cells in order for them to become malignant (Shay and Wright, 2005). This means that if cells lack sufficient DNA damage responses, such as in the case of mutated p53, the cells could bypass senescence and become genetically unstable. This second checkpoint is known as "cellular crisis" (Figure 1.4). "Cellular crisis" is characterised by critically short telomeres and chromosome instability, which can lead to telomere fusions (Capper

et al., 2007). In order for cancer cells to continue proliferating at this stage, telomeres must either be maintained by the upregulation of telomerase (and therefore increased telomerase activity), or through alternative lengthening of telomeres (ALT) (Bryan and Reddel, 1997). ALT is recombination based and is utilised by approximately 10% of cancers, whereas telomerase upregulation can be found in up to 90% or cancers. This makes telomerase activity an interesting prospect for anticancer treatment (Kirkpatrick et al., 2003).

### 1.2.4 Telomerase

The telomerase enzyme is a ribonucleoprotein consisting of multiple subunits, two of which are essential. These subunits perform the main function of the enzyme, by maintaining telomere length. The human telomerase RNA component (hTERC) functions as an RNA template for the human telomerase reverse transcriptase component (hTERT), which adds the telomeric repeats to the ends of telomeres (Figure 1.5) (Carlin et al., 1997). This makes hTERT the limiting factor for enzyme activity (Sheng et al., 2013). It has even been shown that the increase of hTERT expression at any stage of the cell cycle results in the immortalisation of the cell line. This is further supported with the fact that hTERT mRNA levels are directly proportional to telomerase activity. Once again, this correlates to the high number of cancers (90%) that have elevated telomerase activity, as they also exhibit increased hTERT mRNA levels (Kirkpatrick et al., 2003).

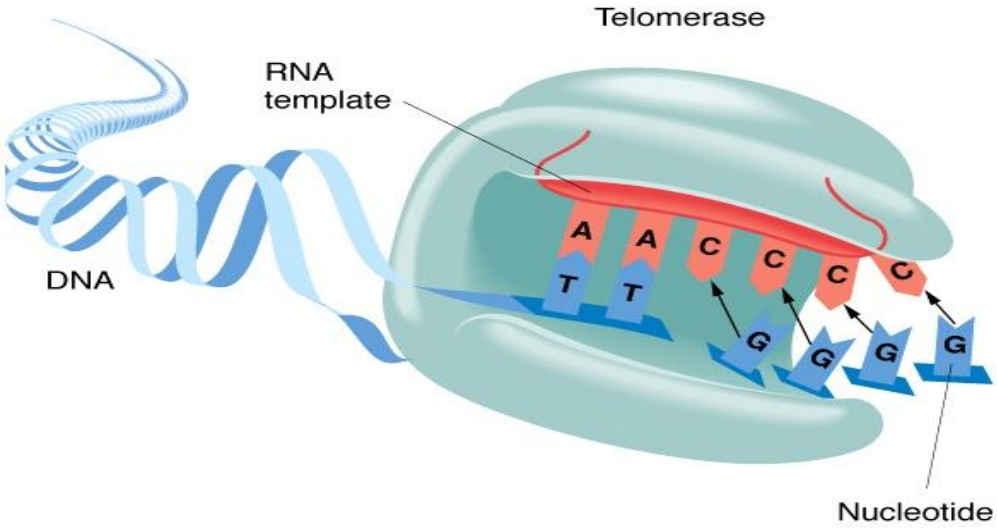


Figure 1.5: Schematic Representation of the Telomerase Enzyme. This diagram shows how hTERT (blue) uses hTERC (red) as a template to add additional telomeric repeats to the ends of chromosomes.

1.2.5 Regulation of hTERT mRNA Expression:

hTERT has been described as the limiting factor of telomerase, as a change in hTERT expression causes a proportional change in telomerase activity (Sheng et al., 2013). Therefore, factors that influence hTERT mRNA expression must be discussed. There are multiple factors such as the variation of the hTERT minisatellite (MNS16A) in addition to mutations of the hTERT promoter sequence, which have both been associated with hTERT expression. Even specific single nucleotide polymorphisms (SNPs) that can be found in the hTERT promoter affect hTERT expression. In addition, an increased risk to lymphoblastic leukaemia and increased hTERT mRNA expression has been linked to the SNP rs2735940 (Sheng et al., 2013).

Similarly, a genetic change in the hTERT minisatellite (MNS16A), which is a polymorphic tandem repeat, downstream of the hTERT gene, has been linked to hTERT expression. It is thought that the antisense MNS16A gene is involved in the silencing of hTERT mRNA. This means that the shorter variant of the minisatellite has an increased ability to silence hTERT mRNA. The larger variants on the other

hand would lead to decreased silencing, due to a decrease in antisense transcription, and therefore cause an increase in hTERT expression (Wang et al., 2003). Further supporting this; the short allele of the variable number of tandem repeats (VNTR) of the MNS16A minisatellite (VNTR-274) has been found to downregulate hTERT mRNA expression (Hofer et al., 2013). This may lead to apoptosis or even senescence. VNTR-274 has even had a suggested protective role against prostate cancer (Hofer et al., 2013). In previous research, it was also found that cell lines containing the larger minisatellite variant had correspondingly high telomerase activity (Bernert, 2014).

Comparably the proto-oncogene, c-myc, has been shown to increase hTERT expression. C-myc directly targets the hTERT gene, leading to increased telomerase activity due to increased hTERT expression (Greenberg et al., 1999; Tang et al., 2016). Even the p53 transcription factor has been known to target the hTERT gene. p53 is thought to directly bind the hTERT gene through the SP1 binding site. This is said to regulate hTERT expression in normal, healthy cells by decreasing hTERT transcription (Kanaya et al., 2000). This however means that if there should be a loss of function mutation in p53, that it could lead to an increase in cell division.

### 1.2.6 hTERT and its Role in the Mitochondria:

Recently it has recently been noted that the multi-subunit hTERT enzyme has multiple functions other than the elongation of telomeres. During times of oxidative stress, hTERT is known to relocate to the mitochondria from the nucleus. This is due to the presence of a targeting sequence specific to the mitochondria (Haendeler et al., 2009). The mitochondrial hTERT has been shown to improve mitochondrial function in times of oxidative stress, suggesting a potential protective role (Saretzki, 2009). Without this form of protection, it could lead to mitochondrial dysfunction, which can further cause the release of reactive oxygen species (ROS). Since ROS are damaging to the genetic material of the cell, increased hTERT protects mitochondrial DNA from damage by binding to the mitochondrial DNA (Haendeler et al., 2009). If the effect of the ROS is severe enough, they can cause the cell to undergo apoptosis or enter replicative senescence. However, since hTERT confers

resistance to ROS, it allows the cell to avoid apoptosis and survive (Saretzki, 2009). Although this may enable the cell to continue functioning, it may have the detrimental effect of allowing the cell to continue proliferating after it has suffered genetic damage. This could potentially lead to "cellular crisis" or even cancer if certain regulatory pathways were to be affected. Studies have found that patients using metformin, an anti-diabetic drug which affects the mitochondria, seem to have lower incidences of cancer (Evans, et al., 2005).

### 1.3 Metformin and Its Role in Cell Proliferation:

Metformin (1,1-dimethylbiguanide hydrochloride), is an antidiabetic drug for type-2 diabetes sufferers. The drug is known to affect the AMP-activated protein kinase (AMPK) pathway. This causes an increase in glucose uptake in muscle cells, which helps mitigate insulin resistance in type-2 diabetes sufferers (Zakikhani et al., 2006). LKB1, a protein kinase and an upstream regulator of the AMPK, is required by metformin to affect the pathway. Additionally, LKB1 has a tumour suppressor function (Evans et al., 2005). The activation of AMPK by metformin causes a signal cascade, which activates the p53 DNA damage pathway. This could indicate that the drug may be able to decrease cell proliferation and therefore potentially reduce the risk of cancer. Indeed, studies have shown that individuals using metformin displayed reduced cancer risk (Evans et al., 2005; Tseng, 2016).

Additionally, it has been shown that cell proliferation in oesophageal squamous carcinoma cell lines is significantly reduced in the presence of metformin (Damelin et al., 2014). Furthermore, it was demonstrated that if mice were treated with metformin in conjunction with conventional chemotherapy, they experienced longer remission times compared to the untreated mice (Hirsch et al., 2009). Metformin treatment also resulted in a decreased recurrence for gastric cancer patients after surgery (Choong-kun et al., 2016). Considering that metformin seems to have an anti-proliferative effect on cancer cells, it may affect certain pathways, such as telomere dynamics, that are involved in cancer progression. Moreover,

hTERT mRNA levels have been shown to be reduced by metformin in endometrial cancer, however the mechanism is not yet understood (Hanna et al., 2012).

The effects metformin has on telomerase activity in oesophageal squamous carcinoma cells have not yet been reported. However, our previous research showed a significant reduction in telomerase activity in an oesophageal cancer cell line expressing wild type p53. (Bernert, 2014). One possible explanation is that p53 represses hTERT expression by acting as a transcription factor and binding the SP1 binding sites found in the hTERT promoter. This would result in a decrease in hTERT expression and therefore a decrease in telomerase activity (Kanaya et al., 2000). This could mean that a p53 mutation would render it unable to directly bind to the hTERT promoter, which results in an increase in telomerase activity and potentially helps to bring about cell immortality. Seeing that hTERT is known to be transported to the mitochondria, and that metformin acts within the mitochondria, by suppressing mitochondrial electron transport which results in the increase of the rate of glycolysis in a p53 dependant manner (Buzzai et al., 2007), there may be a direct interaction between the drug, hTERT and p53.

### 1.4 Telomerase Activity Assays:

Many different telomerase activity assays have been developed, these are often based on the telomeric repeat amplification protocol (TRAP). A TRAP protocol consists of a DNA telomerase substrate which is amplified by the telomerase enzyme in the presence of NTPs (reviewed in Zhou and Xing, 2012). After an extraction process, the enzyme extends the telomeric repeats on the substrate, which can be quantified by a quantitative polymerase chain reaction (qPCR). The number of repeats added is directly proportional to the signal obtained, which is then an accurate measurement of telomerase activity. TRAP based telomerase activity assays are usually reliable, however they can present many different problems. These protocols require whole protein extract from tissues or cells, which can leave impurities behind. Due to the sensitivity of the DNA binding dyes and fluorescent probes utilised by these protocols, these impurities, such as cell debris and genetic

material, can adversely affect the experiment. As with most PCR based techniques, non-specific binding and the formation of primer dimers can lead to false positives (reviewed in Zhou and Xing, 2012). qPCR based techniques are also often expensive and time consuming. Nanoparticles could be an answer to many of these problems.

There are many different types of nanoparticles with unique and interesting properties. Quantum dots (QDs) for instance have been previously used to detect telomerase activity. One of the characteristics of QDs is that the colour of the particle changes with its size. The colour shifts towards blue, the smaller a QD becomes. In this telomerase activity protocol, the enzyme adds telomeric repeats to a DNA telomerase substrate, during which Cy5-dATPs is also incorporated. A newly synthesised DNA strand is then hybridised to a biotinylated capture probe, which allows for the binding of streptavidin-coated QDs. The QDs are then exited using light at 488nm wavelength, which causes fluorescence resonance energy transfer to the Cy5 receptor causing a fluorescent signal. Subsequently, the number of Cy5 can then be measured. The number of Cy5 is directly proportional to the length of the newly synthesised strand, as the Cy5 have consistent spacing between one another (due to the adenine residues found in telomeres). Telomerase activity can then be estimated by measuring the number of Cy5 through internal reflection fluorescence microscopy (Zhu et al., 2015).

Metallic nanoparticles, for example gold nanoparticles (AuNPs) are another type of nanoparticle that have very interesting optical properties. Similar to QDs, AuNPs change the colour of the nanoparticle colloid solution based on their size and proximity to one another (Yarbakht and Nikkhah, 2016). The larger the AuNPs are in solution, the more the colour of the solution will shift towards the blue. On the other hand, the smaller the AuNPs in the solution, the more red shifted the colour of the solution becomes. If AuNPs become more aggregated, the colour of the solution also shifts towards blue. This aggregation can be achieved by adding salt to the AuNP solution, which cause the AuNPs to stop repulsing each other and begin to interact with one another. Due to these properties, one could very easily detect changes to the surface of the nanoparticle, as even a small change could result

in an observable colour change (Yarbakht and Nikkhah, 2016). This sensitivity as well as their ability to be easily functionalised to many different molecule, including thiolated DNA (by covalent bonding), could make AuNPs a very useful biosensor in detecting telomerase activity. If AuNPs could be coupled to a telomerase substrate (thiolated DNA), and salt is added to the solution, the colour of the solution would shift towards blue due to the close association of the particles. However, once telomerase is allowed to elongate the substrate, the steric hindrance caused by the elongated DNA, and possible secondary structure formation, will prevent the nanoparticle from closely associating. This would cause the colour of the solution to shift from blue to a more red colour (Wang et al., 2012) (Figure 1.6). This colour change could then be measured using UV-visual spectrophotometry (Zhang et al., 2012).

Detecting telomerase activity using nanoparticles could prove very beneficial, as many steps found in conventional qPCR based methods could be eliminated. This includes the use of fluorescent probes and dyes, which can easily degrade, resulting in differing results from one experiment to another. This would also mitigate signal bleed through in 96-well plates, which can result in false positive results. Nanoparticles can reduce the time and cost involved in performing telomerase activity assays. For example, telomere extension has been detected in the protein extract of only 10 HeLa cells using AuNPs (Wang et al., 2012). Here Wang et. al confirmed telomerase inhibition, and therefore decreased elongation of the coupled (DNA) telomeric substrate, by TMPyP4 using their gold nanoparticle assay.

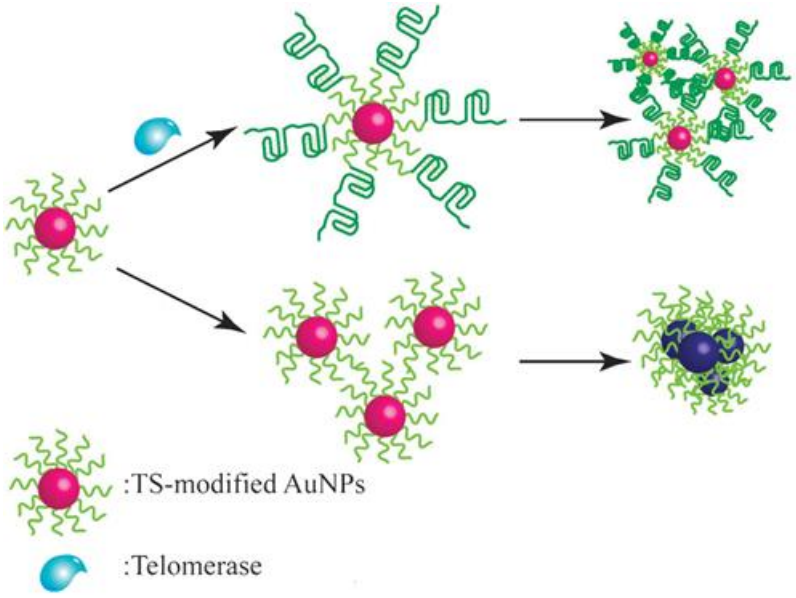


Figure 1.6: Principles of a AuNP Based Telomerase Activity Assay (adapted from Wang et al., 2012). This illustration shows thioalted DNA (telomerase substrate) functionalised AuNPs. After functional telomerase is introduced to the nanoparticle solution, the substrate is elongated. This causes steric hindrance between the particles, causing them to disperse and causes a red shift in colour. The nanoparticle solution with the non-elongated substrate turns a blue colour due to the close association of the nanoparticles.

## 1.7 Aim:

To improve on a nano-particle based detection method for telomerase activity and thereafter determine the effect of metformin on telomere dynamics in Oesophageal squamous carcinoma cells.

### 1.7.2 Objectives:

1) Determine the effects of metformin on cell proliferation by performing MTT assays.

2) Determine hTERT mRNA expression in metformin treated and untreated cells by qPCR.

3) Assess telomere length in metformin treated and untreated cells by qPCR.

4) Assess telomerase activity in metformin treated and untreated cells by qPCR.

5) Optimize chemical synthesis of spherical silver, platinum and gold nanoparticles by metal salt reduction under strict pH and temperature controls.

6) Characterise nanoparticle size and morphology using UV spectrophotometry and electron microscopy.

7) Functionalise nanoparticles with thiolated DNA and confirm successful functionalisation using electron microscopy.

8) Detect telomerase activity on functionalised nanoparticles using UV spectrophotometry and compare it to conventional qPCR-based methods.

## 2 Materials and Methods:

### 2.1 Cell Culture:

#### 2.1.1 Cell Culture Protocol:

Oesophageal carcinoma cell lines; WHCO1, WHCO5 (Veale and Thornley, 1989), lung fibroblast; MRC5 (JACOBS et al., 1970), SNO (Bey et al., 1976), and human embryonic kidney cells; HEK293 (Graham et al., 1977), were cultured for this project. Professor R. Veale of the cell biology laboratory, at the University of the Witwatersrand, South Africa kindly provided the oesophageal cancer cells. Both WHCO1 and SNO cell lines were utilised in our previous work (Bernert, 2014). Inclusion of these cell lines was to verify the previously obtained data. HEK293 cells were used to optimise procedures involving telomerase activity and hTERT expression, as these cells are known to display relatively high levels of hTERT and telomerase activity (Letsolo et al., 2010). The MRC5 cell line on the other hand was used as negative control as it expresses very little to no telomerase activity. Ethics approval was obtained from the Human Research Ethics Committee (Medical): reference number W-CJ-140804-1.

Each of the five cell lines were cultured in 88% Dulbecco's Modified Eagle's Medium (DMEM) containing 10% Foetal Calf Serum, 1% Penicillin-Streptomycin and 1% L-Glutamine. The cells were kept in a 5% $CO_2$, 37 °C humidified atmosphere to ensure that the pH of the system remained constant through the $CO_2/HCO_3$- buffering system and that the cells experienced maximum cell growth.

Each cell culture flask was viewed under an inverted light microscope to monitor cell growth, cell detachment and to determine the level of confluency. After the cells reached approximately 80% confluency, they were harvested and passaged to prevent contact inhibition and therefore allow the cells to continue growing. To passage the cells, the cells were first detached from the flask through trypsin-EDTA treatment. The trypsin-EDTA was then inactivated by adding an equal volume of cell culture medium. The cells were then evenly passaged into multiple culture

flasks. The cells were treated with metformin while the untreated controls were cultured alongside the treated cells.

After harvesting, some cells were cryopreserved to be used at a later stage. After trypsinisation the cells were harvested and centrifuged at low RPM (±200-400 g) for 10 minutes. The excess media was then removed and the pellet resuspended in a cryopreserving solution (15% Glycerol, 20% FCS, 65% DMEM). The vials were then kept at -20 ˚C overnight and then transferred to -80 ˚C or liquid nitrogen storage. When thawing the frozen cells, an initial high FCS concentration of 20% was used to provide extra nutrients for the cells. This was then stepped down to 10% once the cells stabilised.

2.1.2 Cell Quantification:

To accurately quantify the number of cells in each flask once they reached confluency, a Neubauer haemocytometer was used. The cells needed to be quantified to ensure subsequent experiments and subcultures utilised consistent numbers of cells for reliable results. To distinguish between dead and live cells, the trypan blue stain was used. This stain is only taken up by dead cells, and is excluded by live cells, which leads to dead cells being stained blue under the microscope (Tran et al., 2011). This allows for easy quantification of unstained, live cells. The stained suspension of cells was diluted and a small sample added to the Neubauer haemocytometer. Live cells were then quantified, using the 16-square region of the haemocytometer, while utilising a light microscope. Thereafter, cell concentration, total number of cells as well as cell viability were calculated using the following formulas:

$$Total\ number\ of\ cells = Cell\ concentration\ \left(\frac{cells}{ml}\right) x\ total\ volume\ of\ suspension$$

$$Cell\ concentration\ \left(\frac{cells}{ml}\right) = cells\ per\ 16\ squares\ x\ 10^4 \text{ x dilution factor}$$

$$Cell\ viability\ (\%) = \left(\frac{number\ of\ viable\ cells}{total\ number\ of\ cells}\right) x\ 100$$

### 2.1.3 MTT Cell Viability Assay

The MTT (3-(4,5-dimethylthiazol-2-yl)-2,5-diphenyltetrazolium bromide) assay was used to determine cell viability. As the metformin treatment may affect cell proliferation and cell viability, this assay is very important to perform. The yellow MTT reagent is added to a plate of cells. Viable cells then reduce the reagent through cellular NAD(P)H-dependent oxido-reductases. This turns the MTT reagent into an insoluble formazan product, which is purple in colour, for 4 hours. The insoluble precipitate is then treated with a detergent and mixed until fully dissolved. After the formazan crystals are dissolved, the solution is read at 600 nm, using a spectrophotometer. The higher the amount of dissolved product, the higher the absorbance reading and therefore the more viable cells are present. This assay was performed in 96-well plates, where each well of a 96-well plate was seeded with 5000 cells. They were allowed to attach overnight and treatment commenced the following day. Each treatment as well as each control was done in triplicate. The controls included the no-cell control, no-MTT control, 100% dead cells (treated with 1% triton-x) as well as the untreated cell control. After the addition of the MTT reagent, the colour change was visualised using DMSO and an ELISA reader. The absorbance readings of the treated samples were then compared to those of the controls.

## 2.2 Nucleic Acid Extraction:

DNA and RNA were extracted from the cells using a modified phenol chloroform method as well as the Quick-RNA MiniPrep Kit (Zymo Research) respectively. In each case the cells were harvested and washed with PBS prior to pelleting them by centrifugation at 10000 g. The pellets were then washed with PBS to ensure no media remained.

### 2.2.1 DNA Extraction:

A modified phenol chloroform extraction method was used to extract DNA from the various cell lines. The extraction buffer was made up of tris, glycerol, SDS and mercaptoethanol. This buffer was used to lyse the cells. Proteinase K was then added to digest the protein. To separate the cell debris and protein from the lysate containing the DNA, isopropanol and phenol chloroform were added to the cell lysate. The solution was then centrifuged at 10000 g for 5min at 4 ºC to pellet the cell debris, leaving the protein in the organic layer. Whilst the aqueous solution was then transferred to a new tube and mixed with ethanol. The solution was then centrifuged at 10000 g for 5min at 4 ºC again in order to precipitate the genomic DNA. Ethanol is then removed by air-drying the DNA pellet prior to resuspending in TE buffer. Both the amount as well as the purity of the DNA was then determined using the Thermo Scientific ND1000 NanoDrop spectrophotometer. After this, the DNA was resolved on a 1% agarose gel to determine integrity.

### 2.2.2 RNA Extraction:

RNA extraction was performed using the Quick-RNA Mini Prep Kit (Zymo Research). The cells were lysed and the protein degraded per the manufacturer's instructions. Cells were lysed using the cell lysate buffer. After a centrifugation step, the supernatant was pipetted into the "spin-away" filter before centrifuging again to remove the majority of the genomic DNA. Ethanol was added to the flow-through and the solution was added to the "Zymo-Spin IIICG Column". After centrifugation, the flow-though was discarded and the column was treated with DNase for 15 minutes to degrade any remaining genomic DNA. After multiple wash steps, the eluted RNA was stored in RNase-free water at -80 ˚C and the yield was determined using a NanoDrop (Thermo Scientific ND1000). As for the DNA, RNA integrity was verified by resolving the samples on a 1% agarose gel.

## 2.3 cDNA Synthesis:

cDNA was synthesised using the ProtoScript First Strand cDNA synthesis Kit (New England BioLabs). The extracted, purified RNA sample was treated with DNase again to ensure that no genomic DNA remained in the sample. A short thermal cycle was then run, where the RNA was incubated at 25 ˚C for 5 minutes, then 42 ˚C for 60 minutes. The reverse transcriptase was then inactivated at 80 ˚C for 5 minutes. The cDNA was then stored at -80 ˚C. Each sample was run alongside a no-template control, as well as a reverse transcriptase negative control to rule out contamination.

## 2.4 Polymerase Chain Reaction (PCR) and Agarose Gel Electrophoresis:

To assess the suitability of the DNA for PCR, MNS16A minisatellite as well as GAPDH and were amplified in all cell lines.

Table 1: PCR Primers

Table 1 illustrates PCR primers that were used in the study

| Primer | 5'-3' Sequence | Region | Reference |
|---|---|---|---|
| MNS16A | F-AGGATTCTGATCTCTGAAGGGTG<br>R-TCTGCCTGAGGAAGGACGTATG | MNS16A Minisatellite | (Wang et al., 2003) |
| GAPDH | F-GTGGACCTGACCTGCCGTCT<br>R-GGAGGAGTGGGTGTCGCTGT | GAPDH | (Zhang et al., 2012) |
| 17pseq1rev | GAATCCACGGATTGCTTTGTGTAC | STELA at 17p telomere | (Britt-Compton et al., 2006) |
| XpYpE | TTGTCTCAGGGTCCTAGTG | STELA at XpYp telomere | (Baird et al., 2003) |
| Teltail | TGCTCCGTGCATCTGGCATC | Telorette tail | (Baird et al., 2003) |
| Telorette2 | TGCTCCGTGCATCTGGCATCTAACCCT | End of telomere | (Baird et al., 2003) |

For all PCR amplifications, KapaTaq Master Mix (Lasec) was used. This PCR master mix contains all the components needed for amplification, such as dNTPs, reaction buffer, magnesium chloride and taq-polymerase. The primers were added separately (Table 1). All amplifications were performed in a MJ Mini thermal cycler (BioRad) using the following thermal cycle: Initial denaturation was performed at 95 ˚C for 2 minutes, followed by 35 cycles of denaturation (95˚C for 30 seconds), annealing (55 ˚C for GAPDH and 56 ˚C for the minisatellite for 30 seconds) and elongation (72 ˚C for 1 minute). A final elongation step was also performed at 72 ˚C for 2 minutes to ensure that all reactions had completed.

After the PCR amplification, samples were resolved on agarose gels, using GRGreen (Inqaba Biotech) as a nucleic acid stain. GRGreen intercalates into DNA and creates a detectable fluoresces signal under UV light. The GAPDH sequence and the MNS16A minisatellite products were resolved on a 2.5% agarose gel. The gels were resolved at 80 V for 45 minutes to separate the DNA fragments by size. A DNA weight marker of known fragment lengths was used in order to determine the size of the amplified samples. The gels were then visualised under UV light.

## 2.5 Quantitative Polymerase Chain Reaction (qPCR):

### 2.5.1 Telomere Length:

Telomere length was determined by using the EvaGreen qPCR System (GeneDireX) as per manufacturer's instructions. EvaGreen is a dye, which fluoresces upon intercalating with DNA. The results obtained from the telomere length qPCR were then compared to that of the 36B4 reference gene to obtain a relative telomere length. The reference gene is a consistent size and can therefore be compared to the telomere length. Relative telomere length can then be determined. The following thermal cycle was used: Initial denaturation consisted of one cycle of 95 ˚C for 10 minutes. Amplification consisted of 45 cycles of 95 ˚C for 10 seconds, 56 ˚C and 58 ˚C (for telomere length and 36B4 respectively) for 10

seconds. The elongation step consisted of 72 ˚C for 10 seconds (where a single acquisition -where fluorescent is measured- was performed).

2.5.2 hTERT mRNA Expression:

hTERT mRNA Expression levels were determined by using the EvaGreen qPCR System (GeneDireX) as per manufacturer's instructions. After cDNA synthesis, samples (including the reverse transcriptase minus controls) were amplified. The relative hTERT mRNA (expected size: 165 bp) expression levels for the different cell lines were determined using the mRNA expression levels of the reference genes (GAPDH and β-globin). The following thermal cycle was used: Initial denaturation consisted of one cycle of 95 ˚C for 10 minutes. Amplification consisted of 45 cycles of 95 ˚C for 15 seconds, 60 ˚C (for GAPDH and β-globin) and 62 ˚C (for hTERT) for 30 seconds and 72 ˚C for 10 seconds (where a single acquisition was performed).

2.5.3 Telomerase Activity:

The TRAPeze RT Telomerase Detection Kit (Merck-Millipore) was used to determine telomerase activity for all cell lines. qPCR amplifies a target DNA strand like conventional PCR, but is also able to simultaneously quantify the synthesis of the DNA strand. This is achieved using a sequence specific primer/DNA probe containing a fluorescent reporter as well as a quencher molecule. These reporter molecules fluoresce; however, due to the proximity of the quencher molecule, the fluorescent signal is suppressed. As the telomerase substrate is elongated by the telomerase enzyme, extracted from the cell lines, the probe causes a complimentary strand to be synthesised by taq polymerase. The incorporation of the probe causes the distance between the quencher and fluorophore to increase, creating a fluorescent signal. Therefore, the fluorescent signal is proportional to the amount of added telomeric repeats. Protein was extracted from cell pellets using 3-[(3-Cholamidopropyl)dimethylammonio]-1-propanesulfonate (CHAPS) lysis buffer and the amount of protein being used was standardised to 0.2 mg/ml obtain reliable data (final concentration of 20 ng/µl). The HEK293 cells were used as a positive

control for telomerase activity (Letsolo et al., 2010). The following thermal cycle was used: Pre-incubation consisted of one cycle of 37 ˚C for 30 minutes and 95 ˚C for 2 minutes. Amplification consisted of 45 cycles of 95 ˚C for 30 seconds, 59 ˚C for 1 minute and 45 ˚C for 10 seconds (where a single acquisition, fluorescent data acquisition, was performed).

## 2.6 STELA Protocol:

The modified single telomere length analysis method (STELA) (Baird et al., 2003) consists of PCR amplification of telomeres extracted from cells. Since telomeres are highly repetitive, some additions and changes must first be made to the standard PCR reaction and Southern blotting procedure. Telomeres were amplified by a procedure where specific primers were first introduced to attach a recognisable fragment, to which the DNA polymerase of the PCR master mix can attach. The primers used in this experiment are described in Table 1 and below (Figure 2.1). Initial denaturation was performed at 95 ˚C for 2 minutes, followed by 35 cycles of denaturation (95 ˚C for 30 seconds), annealing (65 ˚C for XpYpE and 59 ˚C for 17p for 30 seconds) and elongation (72 ˚C for 5 minute). A final elongation step was also performed at 72 ˚C for 10 minutes to ensure that all reactions had completed. After the amplification of the telomeres, the PCR products were resolved on a 0.8% agarose gel at 120 V for 12 h. After the desired DNA fragments were separated, the DNA fragments within the gel were transferred onto a sheet of nitrocellulose. These fragments were then hybridised with a specific probe that is complimentary to the target sequence, which helps identify the fragment of interest. The agarose gel was placed on soaked filter paper in the presence of a transfer buffer, on top of which a nitrocellulose membrane was placed. More soaked filter paper was then placed on top of the nitrocellulose membrane. Weights were then added to the resulting stack to ensure that the DNA transfer proceeded evenly (Sambrook et al, 1989). During the transfer, the negatively charged DNA attaches to the positively charged membrane. The newly attached DNA was then fixed to the membrane by UV light exposure. The membrane was then treated using the TeloTAGGG kit (Roche). This

treatment allows for the visual detection of single telomeres on the membrane. The now attached single telomeres were then hybridised with a digoxigenin (DIG)-labelled probe. After this, an alkaline phosphatase coupled anti-DIG antibody is bound to the DIG probe, which allows for the visualisation of the telomeres through the addition of a chemiluminescent substrate. This substrate reacts with alkaline phosphatase, resulting in a detectable colorimetric signal. This was then visualised using a ChemiDoc (BioRad). The standard STELA procedure utilises radio labelled-probes (Baird et al 2003).

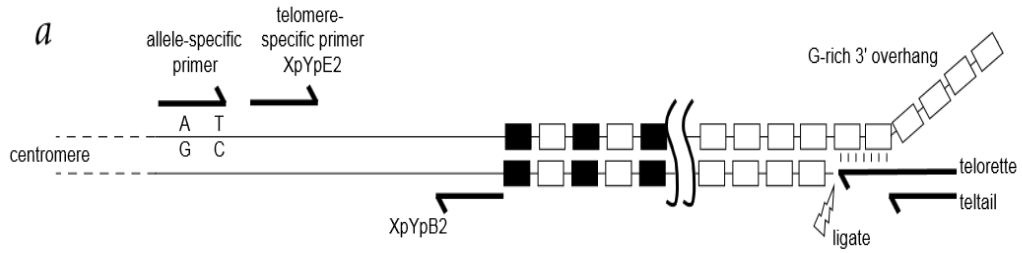


Figure 2.1: Graphic Representation of STELA Primer Binding Dynamics (modified from Baird et al., 2003). This diagram shows the primer binding locations of the STELA technique involved in the extension of the telomeres.

## 2.7 Nanoparticle Synthesis:

The synthesis and functionalisation of the nanoparticles were performed in the laboratory of and under the mentorship of Dr Sharon Moeno at the Department of Oral medicine, University of Witwatersrand. After synthesis, the nanoparticles were attached to synthetic thiolated DNA which, in this case, was a substrate for extracted telomerase to extend.

### 2.7.1 NP Synthesis Procedure:

A concentrated 3:1 mixture of HCl:$HNO_3$ was used to treat the glassware. This prevented nanoparticles (NPs) from attaching themselves to the sides of the glassware. Silver, Gold and Platinum NPs were synthesised by the metal salt reduction method (ions sourced from chloroauric acid, silver nitrate and chloroplatinic acid respectively), using sodium citrate as the reducing agent. Deionised water (50 ml) was added to a treated glass beaker. Metal salt was then added to the beaker to a concentration of 1mM. The beaker was then placed on a hotplate. The solution was stirred and allowed to heat up. Temperature is a vital factor in nanoparticle synthesis, so multiple were used to find the optimum temperature for each metal salt. Once the solution reached the desired temperature, sodium citrate was added until a colour change occurred. The amount and method of addition of the reducing agent also affects the formation of the NPs so multiple concentrations, and methods (ie. dropwise or rapid addition) were tested. The presence of a crimson colour indicated the formation of AuNPs within the desired size range, whereas brown and dark yellow indicated the synthesis of silver and platinum NPs respectively. The solution was then removed from the heat source and allowed to settle for a further 20 minutes with gentle stirring. The size and morphology was then verified using both scanning and transmission electron microscopy (SEM and TEM) as well as UV-visual spectrophotometry and Zetasizer measurements (light scattering). The NPs were then stored at room temperature in the dark.

### 2.7.2 Platinum Nanoparticle Protein Functionalisation

Platinum nanoparticles were first bound to lysozyme as a proof of concept that functionalisation of nanoparticles would result in a change in the UV-visible spectrum, as well as observe any changes under the SEM and TEM. Platinum nanoparticles were selected as they were thought to have a better chance to interact with the amide group found on the protein. The protein was added to 5 ml of diluted platinum nanoparticles (to a final concentration of 30 ng/µl). The nanoparticle-protein solution was then incubated for 1h at room temperature while being stirred.

The absorbance of the protein-nanoparticle solution was quantified by spectrophotometry (UV-1800 Spectrophotometer (Shimadzu)) and the size and shape of particles were verified by SEM and TEM.

### 2.7.3 AuNP DNA Functionalisation:

All glassware was treated with 12M NaOH and washed with deionised water to prevent AuNPs from attaching to the glass, as this may affect the yield of the functionalised nanoparticles. Thiolated DNA (1 mM thiolated DNA: 5'-$HS(CH_2)_6$TTTTTTTTTTAATCCGTCGAGCAGAGTT-3' (Wang et al., 2012)) was bound to both gold and platinum nanoparticles using a pH dependant sodium citrate method alongside a simple incubation. This was to improve on the method put forward by Wang et. al 2012, as the functionalisation reaction was labour intensive and time consuming, requiring constant adjustment and taking up to 40h to complete. For the sodium citrate method, the thiolated DNA was added to the nanoparticle solution to a final concentration of 2 µM and was mixed by inversion. The pH-buffered sodium citrate solution was then rapidly added to the mixture to a final concentration of 10 mM and was incubated for 20 minutes at room temperature. For the simple incubation method, the nanoparticle solution was once again brought to a final concentration of 2 µM of thiolated DNA. The solution was then mixed by inversion for 16h to allow the nanoparticles to attach to the thiolated DNA. The absorbance of the functionalised particles was read on the UV-vis spectrophotometer along with a control solution containing no DNA. The DNA modified AuNPs were then centrifuged at 13000rpm for 45 minutes to remove any excess DNA (Wang et al., 2012). The modified AuNPs were then resuspended in deionised water.

### 2.7.4 AuNP Based Telomerase Activity Assay:

The telomerase activity assay was based on the procedure by Wang et. al 2012, with the aim of increasing the speed at which the assay was performed as well as the ease of reading the results. In addition, Wang et. al 2012 performed their experiment

on Cervical cancer (HeLa), liver carcinoma (HepG2) and (breast cancer (MCF7), leukaemia (K562) cell lines. The aim was then to create a rapid, easy to use test which could measure telomerase activity in oesophageal cancer cell lines. The AuNP based telomerase activity assay was designed to be similar to a PCR reaction. A buffer was added to the DNA functionalised nanoparticle solution containing essential components needed by the telomerase enzyme to elongate the telomeric DNA substrate (20mM Tris-HCL at pH8.3, 6.3 mM KCL, 1 mM EGTA, 0.005% Tween-20, 0.1 mg/ml BSA, 1.5 mM $MgCl_2$, 1 mM dNTPs) (Wang et al., 2012). Protein extract (extracted using CHAPS lysis buffer as described in 2.5.3), from HEK293 cells, was then added to the solution to a final concentration of 20 ng/µl, to keep it consistent with the qPCR telomerase activity assay. The solution was then incubated at 45 ˚C for up to 2h. This differed from the protocol designed by Wang et. al 2012; to ensure that the DNA was significantly elongated, 2h incubation was used instead of the 1h incubation and the temperature was changed from 30 ˚C to 45 ˚C to keep it in line with the temperatures used in the qPCR based telomeres activity assay. After the extension reaction, the solution was transferred directly to a 96-well plate and the absorbance was read in an ELISA reader at 530 nm. This wavelength was chosen as it was determined to be the peak absorbance for the AuNP solution used in this experiment. This was an attempt to decrease the time and steps required to measure the absorbance compared to the method described by Wang et. al 2012, where they utilised a 400–750 nm spectra. The assay was then performed on SNO and WHCO5 cell lines due to the results obtained from the TRAPeze kit. Changes in the absorbance of the samples were then compared to the results obtained from the qPCR telomerase activity assay. A decrease in absorbance should indicate a decreased telomerase activity, as the nanoparticles associate closer together (Yarbakht and Nikkhah, 2016). This could then be compared to the decrease found with the TRAPeze qPCR kit.

### 2.7.5 Electron Microscopy (SEM and TEM)

Scanning electron microscopy (FEI Quanta FEG-SEM) and transmission electron microscopy (FEI Spirit 120 kV TEM) were used to determine the shape and size of

the synthesised gold, platinum and silver nanoparticles. Similarly, the lysozyme-conjugated platinum nanoparticles as well as thiol-DNA conjugated gold nanoparticles were viewed under SEM and TEM. Sample preparation for the SEM included adding liquid nanoparticle solution to a carbon film attached to a sample stub. The sample was then dried to ensure that no liquid remains, as this could adversely affect the vacuum within the microscope. Sample preparation for the TEM included adding liquid nanoparticle solution to a 3 mm diameter copper grid coated with lacey carbon. The sample was then dried under a heat lamp until no moisture remained. The nanoparticles would then remain trapped on the lacey carbon.

## 2.8 Data Analysis and Statistical Evaluation:

The data collected from these experiments were analysed and evaluated in Microsoft Excel and GraphPad Prism (v6.05). Normalising as well as sorting in the obtained data was done in Microsoft Excel, whereas the statistical analysis was performed in GraphPad Prism, using ordinary one-way ANOVA at 95% confidence level between all sample groups.

# 3 Results:

## 3.1 Cell Viability and Metformin Treatment:

HEK293, MRC5, SNO, WHCO1 and WHCO5 cell lines were successfully cultured and treated with 5 and 10mM metformin for up to 72 h. Increased cell detachment was observed at these metformin concentrations after 48 and 72 h, compared to the untreated controls which had little to no detachment. The MTT assay was performed on each cell line to determine if metformin affected cell viability. Equal number of cells (5000) were added into each well of a 96-well plate. The cell lines were treated for 48 and 72 h with 5 and 10 mM metformin. No significant difference in cell viability was seen for the HEK293, MRC5, SNO and WHCO1 cell lines (Figure 3.1 A-D). The WHCO5 cell line (Figure 3.1 E) however showed a significant reduction in cell viability, compared to the untreated control, for both the 48 h and 72 h treatments.

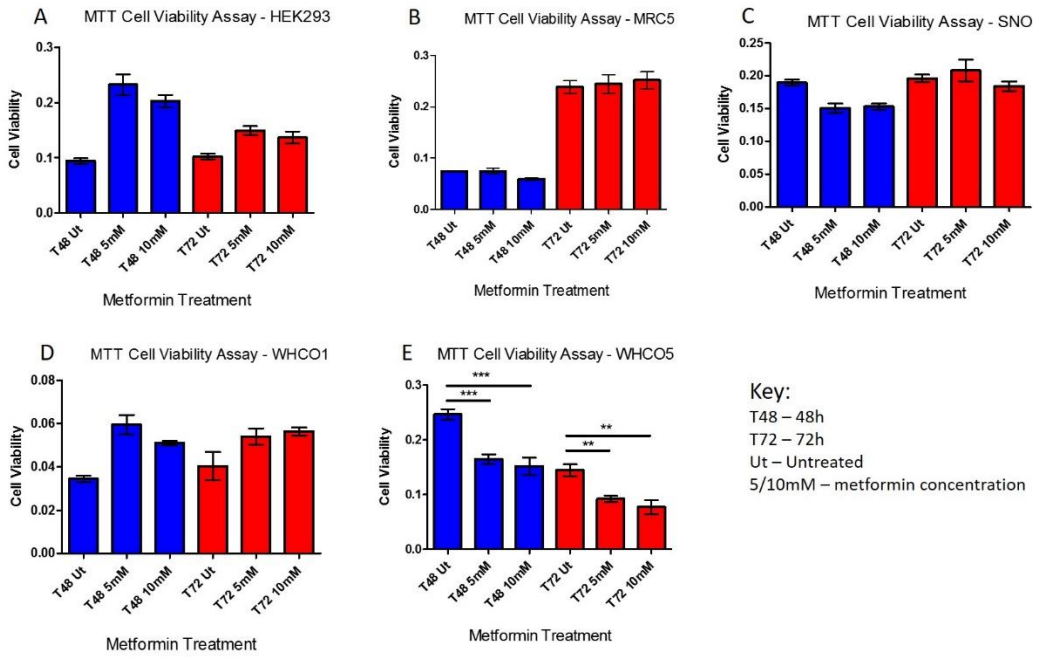


Figure 3.1: Effects of Metformin on Cell Viability in HEK293, MRC5, SNO, WHCO1 and WHCO5 Cells. An MTT assay was performed on the HEK293 (A), MRC5 (B), SNO (C) and WHCO1 (D) and WHCO5 (E) cell lines. Each cell line was treated with 5 and 10 mM metformin for up to 72 h and compared to an untreated control at a 95% confidence level (where $^{**}P \leq 0.01$ and $^{***}P \leq 0.001$).

## 3.2 Single Telomere Length Analysis (STELA):

The modified STELA was performed; however, the GR-Green nucleic acid stain produced no visible bands in the agarose gel after viewing it under UV light. Subsequently, no bands were visible, after the transfer to the nitrocellulose membrane. This may have been due to the nitrocellulose membrane being expired. Due to these complications as well as the high cost of the membranes, it was decided to determine telomere length using qPCR.

## 3.3 Telomere Length:

Telomere length was determined using qPCR. The telomere length reading was compared to that of the 36B4 reference gene to obtain a relative telomere length

(Pusceddu et al., 2015). This was unfortunately only successful in the SNO and WHCO5 cell lines, as the other samples would not amplify. The qPCR results were analysed in GraphPad Prism using ordinary one-way ANOVA at 95% confidence level to compare each data set. In the SNO cell line a significant decrease in telomere length was observed after the 72 h treatment at both the 5 and 10 mM metformin concentrations (Figure 3.2 A). The WHCO5 cell line on the other hand showed a decrease in the 48 h treatment for both 5 and 10 mM metformin concentration (Figure 3.2 B). It is also notable that there is a non-significant decrease in the 72 h 5 mM treatment, which could indicate that the 10 mM 72 h sample is an outlier.

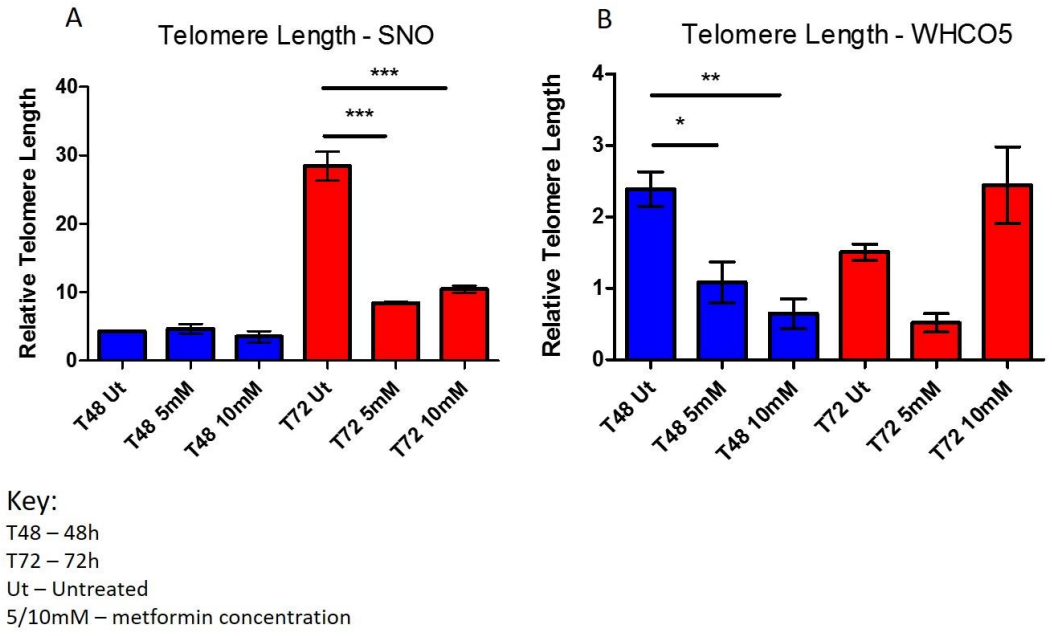


Figure 3.2: Effects of Metformin on Telomere Length in SNO and WHCO5 Cells.
Telomere length was determined using qPCR on 5 and 10 mM metformin treated SNO (A) and WHCO5 (B) cell lines. This was then compared to the 36B4 reference gene (where $^{**}P \leq 0.05$, $^{**}P \leq 0.01$ and $^{***}P \leq 0.001$).

3.4 hTERT mRNA Expression:

hTERT mRNA expression was determined by comparing the hTERT expression qPCR results to that of the reference gene; GAPDH. β-globin was also used as a reference gene; however, no amplification was obtained and could therefore not be compared to the expression results. Due to the expense of the qPCR reagents as well as the large number of samples that had to be analysed per cell line (each sample in triplicate for each of the two reference genes as well as the hTERT gene), the analysis was performed on the WHCO5 cell line only (Figure 3.3). This was due to the cell line showing both a significant decrease in telomere length as well as cell viability due to the metformin treatment. qPCR analysis showed no significant difference in hTERT mRNA expression for the treated and untreated WHCO5 samples

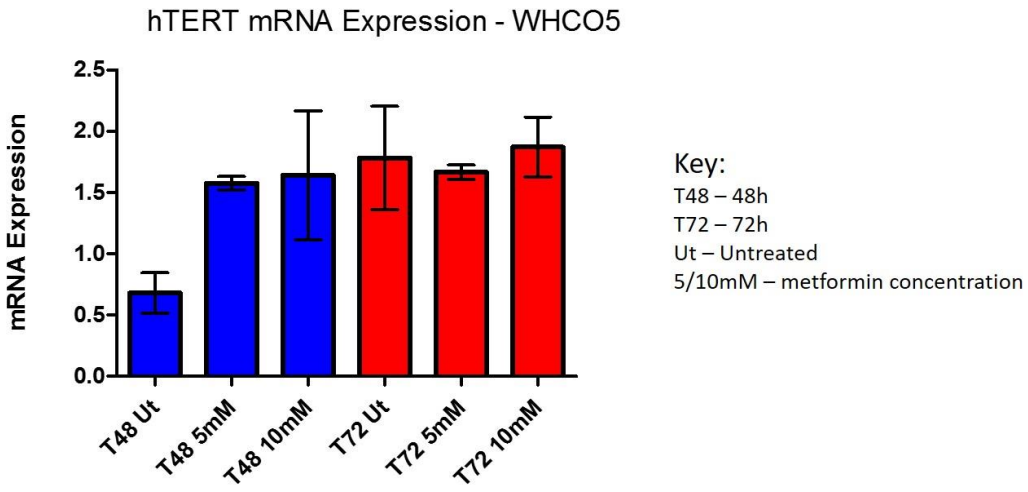


Figure 3.3: Effects of Metformin on hTERT mRNA Expression in WHCO5 Cells.
mRNA expression was determined in the WHCO5 cell line using GAPDH as a reference gene. No significant difference was seen in both the 48 and 72 h treatments compared to the untreated control.

3.5 Telomerase Activity by qPCR:

The TRAPeze RT Telomerase Detection Kit (Merc) was used to determine telomerase activity by qPCR. Telomerase activity was measured in all cell lines, using the HEK293 cells as a positive control and the MRC5 cell line as a negative control. Statistical analysis was performed through GraphPad Prism, using ordinary one-way ANOVA at 95% confidence level to compare the metformin treated and untreated samples. Only the 48 h readings were obtained for both the WHCO1 and WHCO5 cell lines, as no amplification took place at the 72 h timepoint (including the untreated control). A significant reduction in telomerase activity was seen in the HEK293 (positive control), SNO and WHCO5 cell lines (Figure 3.4 A, C, E) with a downward trend seen in the WHCO1 cell line (Figure 3.4 D). The MRC5 cell line (Figure 3.5 B) showed little to no telomerase activity, which was expected from a negative control, however the 72 h untreated MRC5 sample seems to be an outlier.

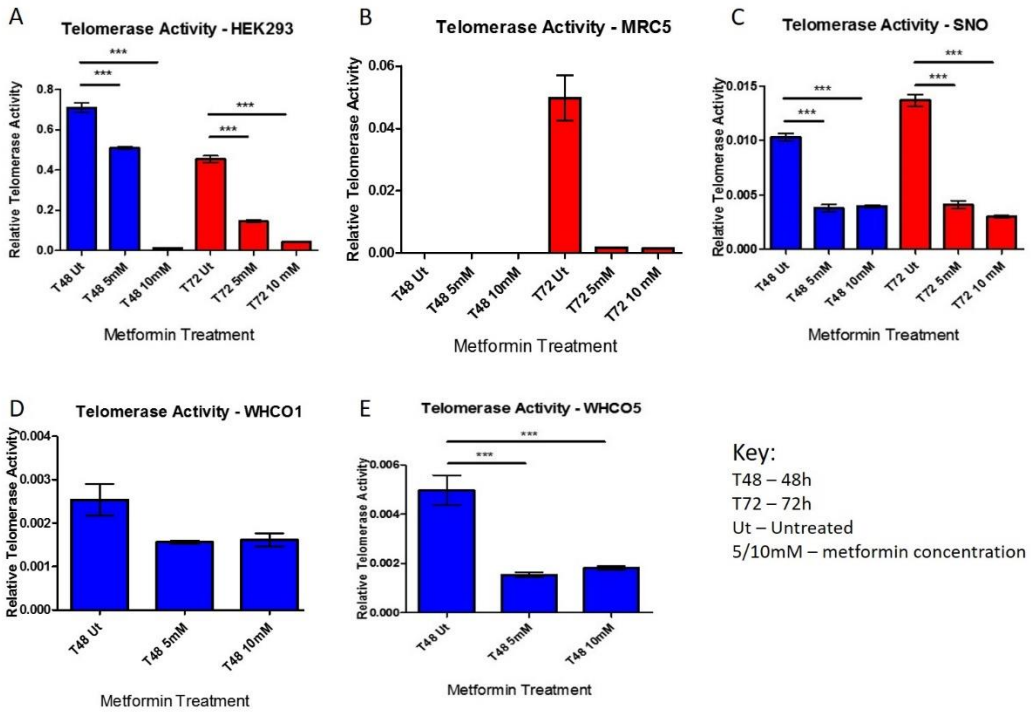


Figure 3.4: Effects of Metformin on Telomerase Activity in HEK293, MRC5, SNO, WHCO1 and WHCO5 Cells. Telomerase activity was determined in the HEK293 (A), MRC5 (B), SNO (C) and WHCO1 (D) and WHCO5 (E) cell lines. Each cell line was treated with 5 and 10 mM metformin for up to 72 h. Statistics were performed at a 95% confidence level (where $^{***}P \leq 0.001$). The MRC5 cell line (B- negative telomerase control) had very low telomerase activity.

## 3.5 Metallic Nanoparticle Synthesis:

Spherical nanoparticles were synthesised using the chemical hydrothermal method by metal salt reduction. Silver nitrate, chloroplatinic acid and chloroauric acid were reduced using sodium citrate to synthesise silver, platinum and gold nanoparticles, respectively. Size and morphology of the nanoparticle were determined using UV-Vis spectrophotometry (Figure 3.5, 3.7), SEM and TEM (Figure 3.6, 3.8, 3.11). ImageJ analysis was performed on the TEM images to determine the average diameter of the spherical nanoparticles. In all three cases, synthesis was successful, however only the gold nanoparticles proved to be of the correct size and uniform morphology needed for most downstream applications (Figure 3.11).

### 3.5.1 Silver Nanoparticle Synthesis:

Silver nanoparticles were successfully synthesised and produced a solution with a brown colour. The spectrophotometry results show a large size range for the silver nanoparticles, as indicated by the wide peak (Figure 3.5). This was further confirmed by the TEM results (Figure 3.6 B), where nano-rods and nano-triangles of varying sizes were present alongside the 50 nm diameter spherical nanoparticles. This large range in particle shapes and sizes would indicate that these silver nanoparticle solutions are not suitable for downstream applications.

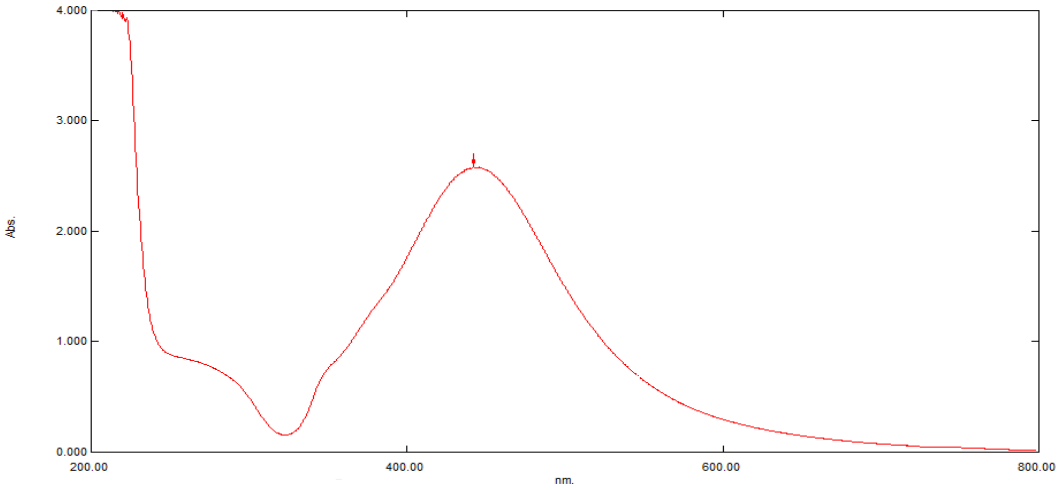


Figure 3.5: Spectrophotogram of a Silver Nanoparticle Solution. The absorbance of the silver nanoparticle solution was measured in the range of 200-800 nm. The spectrophotogram shows one wide peak at 450nm which has shoulder at 340 nm. This is indicative of a large size range of the silver nanoparticles.

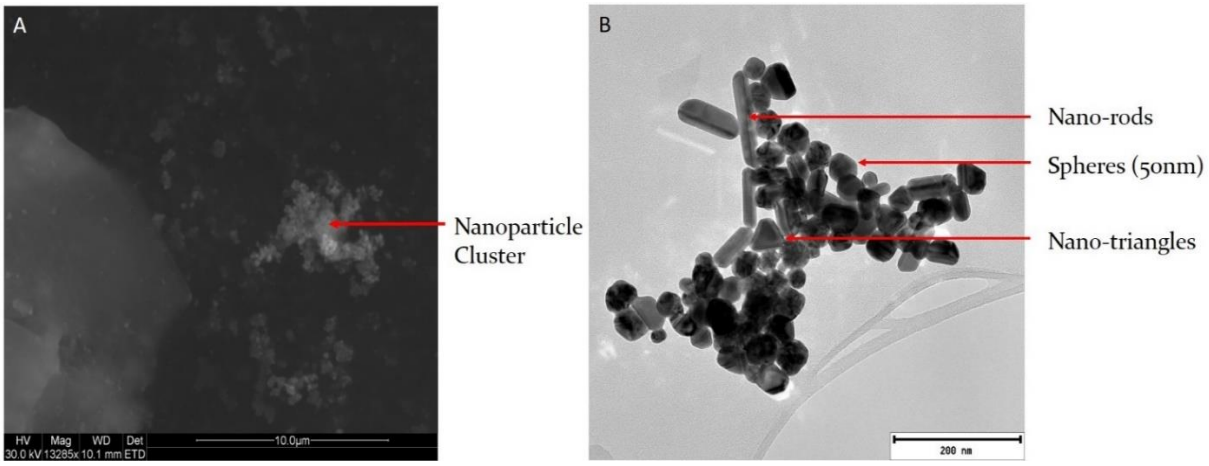


Figure 3.6: Synthesis of Silver Nanoparticles. SEM and TEM images of the silver nanoparticles were taken. The SEM image (A) showed clusters of nanoparticles. However, the TEM image (B) showed the presence of nano-rods and nano-triangles in the nanoparticle solution as well as an average spherical particle size of 50 nm.

3.5.2 Platinum Nanoparticle Synthesis:

Platinum nanoparticles were synthesised, producing a solution with a dark yellow colour. The Spectrophotogram (Figure 3.7) showed no distinct peak, making it difficult to determine the uniformity of the platinum nanoparticles. Indeed, it was thought that synthesis was not successful, however SEM and TEM images (Figure 3.8) confirmed the presence of nanoparticles. The TEM image (Figure 3.8 B) showed that the particles were very closely associated and therefore a more accurate ImageJ analysis was not possible.

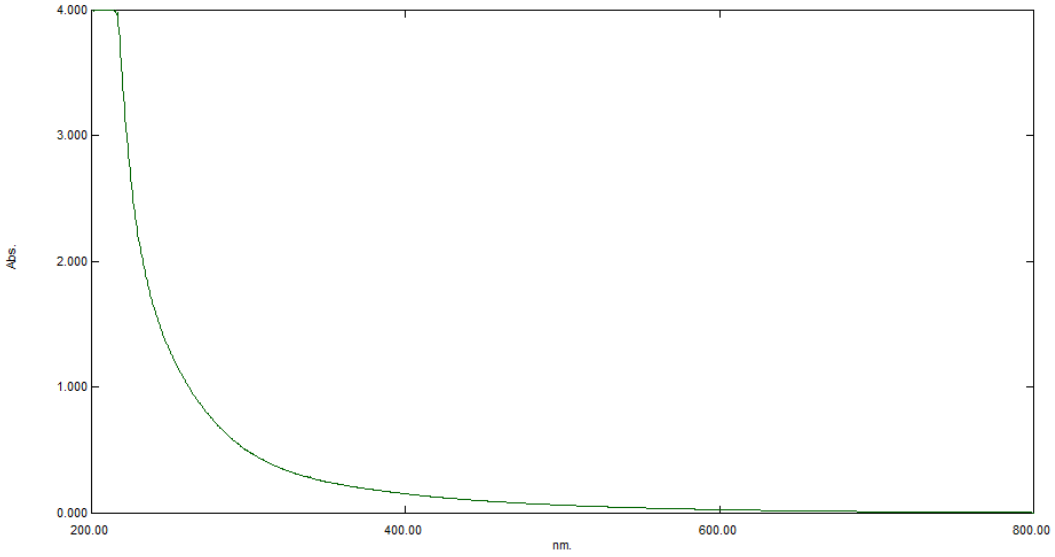


Figure 3.7: Spectrophotogram of a Platinum Nanoparticle Solution. The absorbance of the solution was measured in the range of 200-800nm. This spectrophotogram showed no distinct peaks.

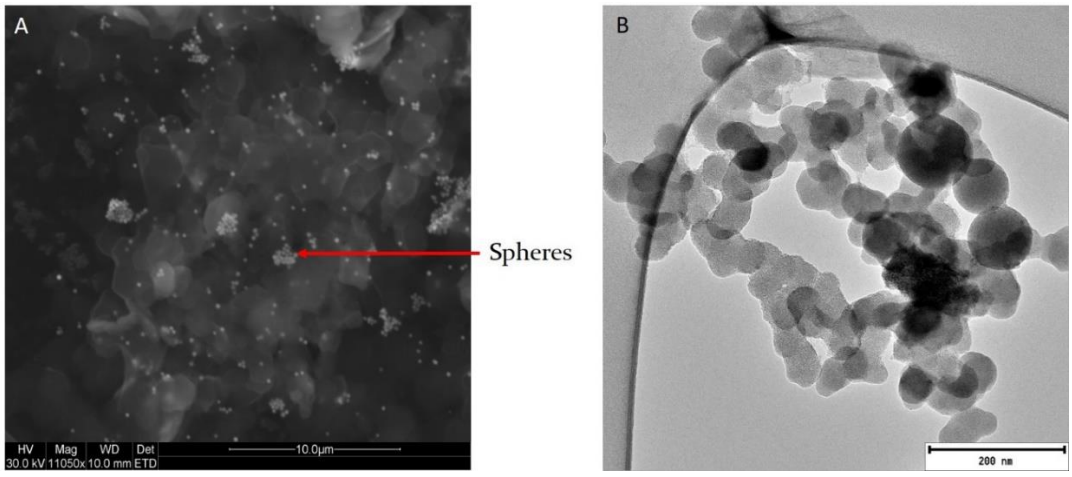


Figure 3.8: Synthesis of Platinum Nanoparticles. Platinum Nanoparticles were successfully visualised under SEM (A) and TEM (B). The particles were clearly visible as large spheres under SEM, however under TEM the particles were very difficult to observe. Under TEM it was seen that the particles were approximately 50 nm in diameter.

3.5.3 Gold Nanoparticle Synthesis:

AuNPs were successfully synthesised and produced a solution with a distinct red colour. The size of AuNPs was also very easy to control, with distinct colour changes accompanying the change in size (Figure 3.9). If the reducing agent was added slowly to the synthesis reaction at 65 ˚C, the colour of the solution turned from red to purple and then blue. The gold tinge in the far-left vial (Figure 3.9) indicates the presence of gold macromolecules/ aggregation. The spectrophotometer readings (Figure 3.10) showed a distinct thin peak, indicating very uniform particle size distribution. This was also confirmed with the TEM images (Figure 3.11 B), where after ImageJ analysis it was found that the average diameter of the particles of the red solution was 13 nm. The narrow size distribution as well as the distinct colour differences due to particle size made AuNPs the natural choice for the subsequent DNA functionalisation.


Figure 3.9: Effects of AuNP Size on Nanoparticle Solution Colour. AuNP synthesis yielded very distinct colour differences as the size of the nanoparticles was increased. As the nanoparticles became larger, the solution underwent a blue shift. A gold tinge is also present in the far-left vial.

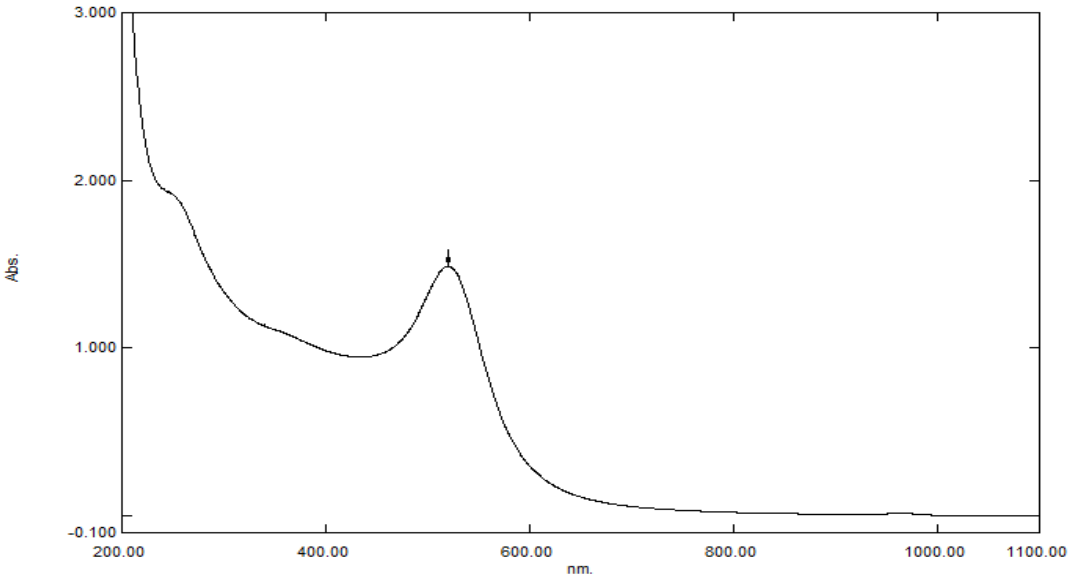


Figure 3.10: Spectrophotogram of a Gold Nanoparticle Solution. The absorbance of the solution was measured in the range of 200-800 nm. A distinct, thin peak can be seen at 530 nm, which may indicate a high degree of uniformity amongst the AuNPs.

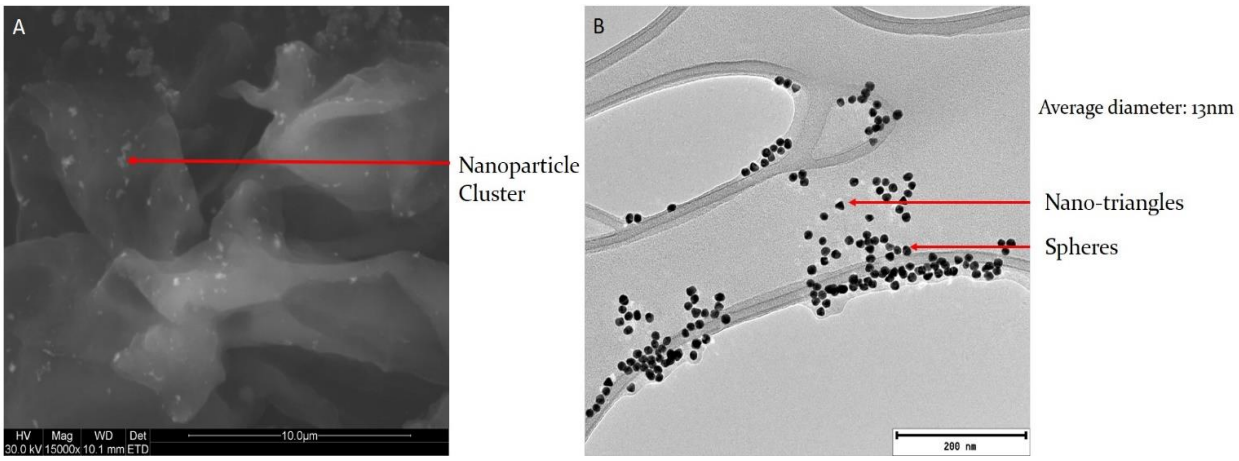


Figure 3.11: Successful Synthesis of AuNPs. The presence of AuNPs was confirmed through SEM (A) and TEM (B). A greater magnification was not possible in the SEM images, due to the resolution of the microscope as well as the small size of the nanoparticles. Under TEM, the nanoparticles were clearly visible and dispersed. The solution consisted mainly of nano-spheres but few nano-triangles were present. ImageJ analysis of the TEM images confirmed that the average diameter of the AuNPs was 13 nm.

## 3.6 Protein Functionalisation of Platinum Nanoparticles:

Platinum nanoparticles were functionalised with lysozyme to determine the effects of surface modification of nanoparticles. Platinum was used due the hope that the thiol groups present in the protein would associate strongly with platinum. The unmodified platinum nanoparticles looked very similar to the lysozyme modified particles, however a possible protein coating was observed (Figure 3.12). Due to the difficulty of viewing platinum nanoparticles under TEM, as well as the lack of a colour change, it was decided to continue the experiment with AuNPs.

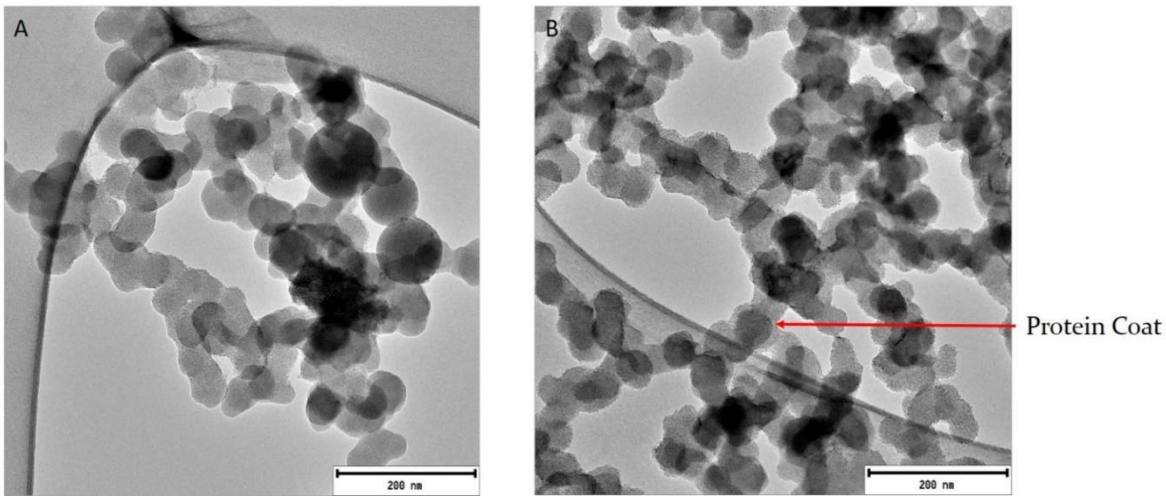


Figure 3.12: Protein Functionalisation of Platinum Nanoparticles. Platinum nanoparticles were functionalised with lysozyme. The un-modified control (A) was very similar to the protein coupled nanoparticles (B). However, some particles seemed to have a coating which may be evidence of the protein attaching to the nanoparticles.

## 3.7 Thiol-DNA Functionalisation of Gold Nanoparticles:

AuNPs were used for subsequent experiments, due to their easily visible colour change in solution as well as their uniformity. Thiolated DNA was coupled to the AuNPs via the simple 16h incubation method. This was preferred, as the sodium citrate buffer method caused rapid aggregation after which the nanoparticles would not re-disperse. DNA coupled AuNPs were then characterised using TEM as well

as spectrophotometry. The spectrophotometer results (Figure 3.13 A) showed a distinct shift after functionalisation. The lowering of the peak could indicate that the particles are more closely associated. This shift is consistent with an increase in size of the modified nanoparticles. (Figure 3.13 B) showed the colour change that occurred due to the functionalisation. This blue shift in colour is once again consistent with larger (or more closely associated) AuNPs. TEM images (Figure 3.14) show a distinct halo around modified AuNPs (B), which cannot be seen in the unmodified particles (A). This halo seems to indicate the presence of DNA on the surface of the AuNPs. Using a Zetasizer (Figure 3.15), the size of the nanoparticles could be determined using light scattering. (A) showed a 40 nm peak suggesting that the average particle size of the AuNP control is 40 nm in diameter. The DNA functionalised sample (B) had two peaks at 40 and 110 nm, suggesting that there are two particle sizes predominantly found in the solution this may be due to some unfunctionalized particles. The sample containing the DNA functionalised AuNPs and the HEK293 protein extract (C) had the two peak sizes (at 40 nm and 110 nm) seen in (B), however there is evidence of massive aggregation (peak from 1000 nm to 6000 nm).

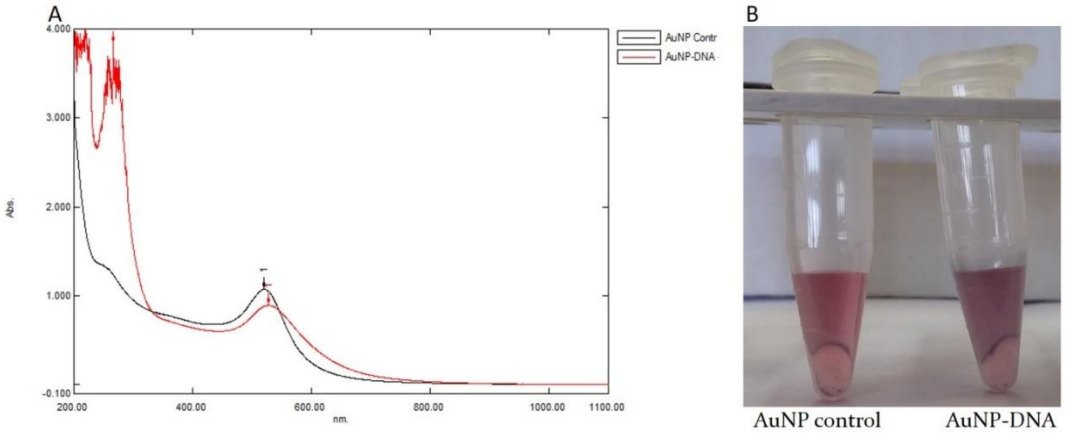


Figure 3.13: Effects of DNA Functionalisation on AuNP Spectrophotogram and Solution Colour. The spectrophotogram of the modified and unmodified nanoparticles (A), where black indicates the control and red indicates the DNA coupled AuNPs, shows a distinct shift in the single peak from 530 nm to 550 nm as well as a lowering of the peak. The red graph also has an additional peak at 260 nm which represents the DNA. (B) shows the colour change that occurred after functionalisation.

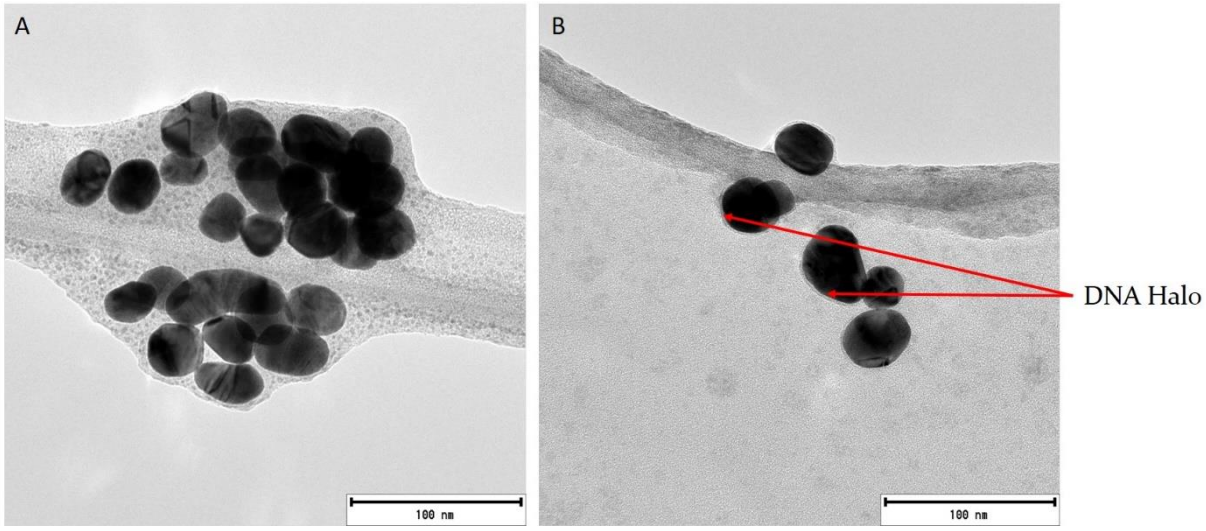


Figure 3.14: Transmission Electron Microscopy Analysis of DNA Functionalised AuNPs. TEM images were taken of the functionalised (B) and non-functionalised (A) AuNPs. A clear halo was seen around DNA modified AuNPs (B), which could not be seen in the unmodified control (A). (Larger AuNPs, approximately 50 nm in diameter were used to show the halo, as the larger halo was more easily distinguishable).

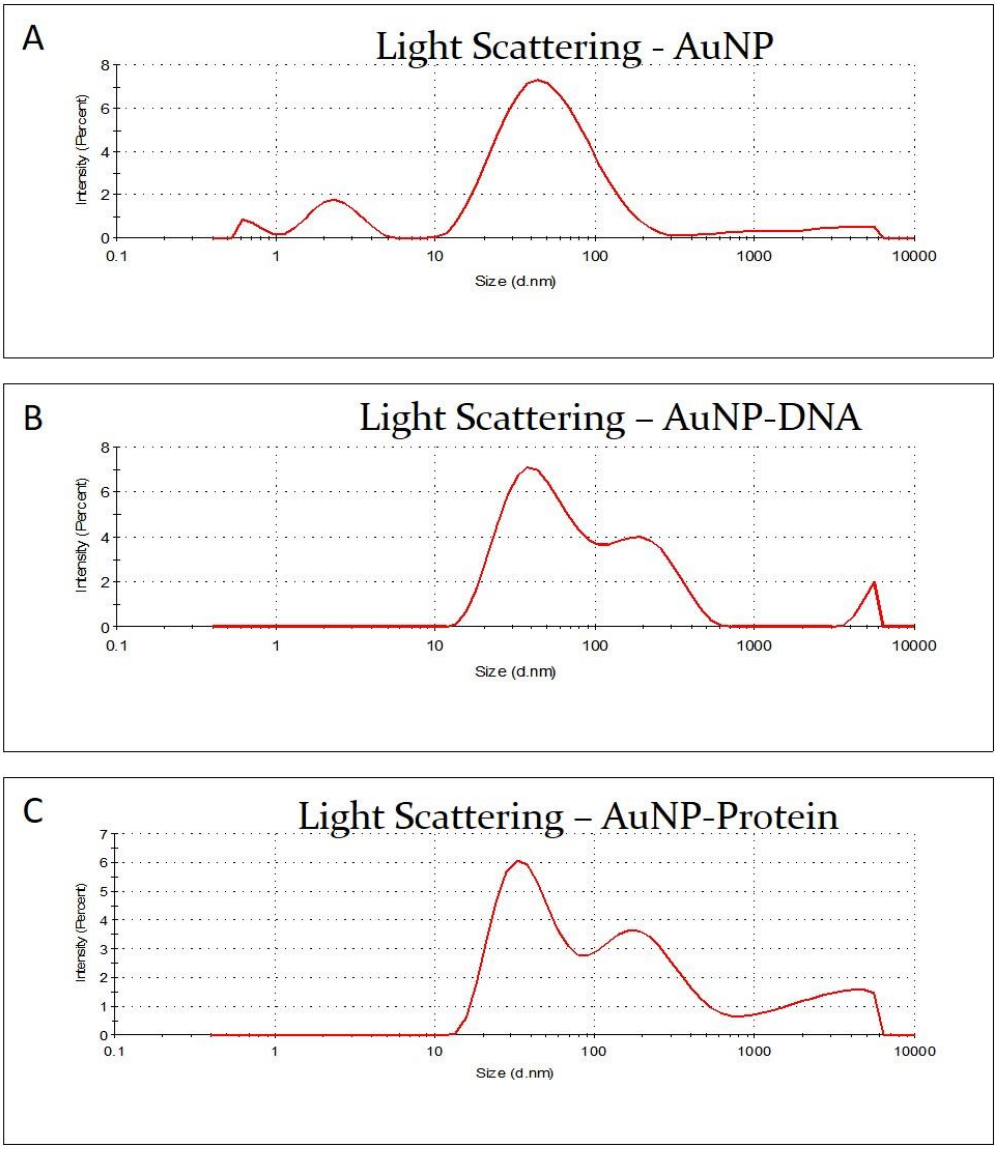


Figure 3.15: Zetasizer Analysis of AuNP Size Distribution using Light Scattering. Zetasizer measurements were taken on the AuNP solution before and after DNA functionalisation. The height of the peak signifies the amount of the standard size of the particles and the width of the peak shows the size deviation from the standard. The unmodified AuNP solution (A) shows a single peak at 40 nm and (B) shows the results of the DNA modified AuNPs, where two distinct peaks, one at 40 nm (as in A) and one at 110 nm can be seen. (C) shows the results of DNA modified AuNPs after the addition of the HEK293 protein extract. The two peak sizes (at 40 nm and 110 nm) are still present, however there is evidence of massive aggregation (peak from 1000 nm to 6000 nm).

## 3.8 Gold Nanoparticles Based Telomerase Activity Assay:

The AuNP based telomerase activity assay was performed similarly to a PCR reaction and the colour change was measured using a spectrophotometer. Thereafter the solutions were viewed under TEM. Although a distinct colour change was seen compared to a negative control (Figure 3.16 C and D), the sample that was allowed to elongate the attached DNA (D) did not show as much aggregation as in (C). This was further confirmed by TEM images (Figure 3.17), where (C) showed massive aggregation compared to (D). this could signify telomerase activity. Once again, this confirms the light blue colour of the sample solution (Figure 3.16-D). The particles in (B) showed slightly more association, which could account for its more purple colour (Figure 3.16-B). After performing the reaction, absorbance readings did not find any significant difference between metformin treated and untreated samples (Figure 3.18) although a difference could previously be seen between elongated and non-elongated samples. Therefore, further optimisation of the assay is required to determine these more subtle differences.

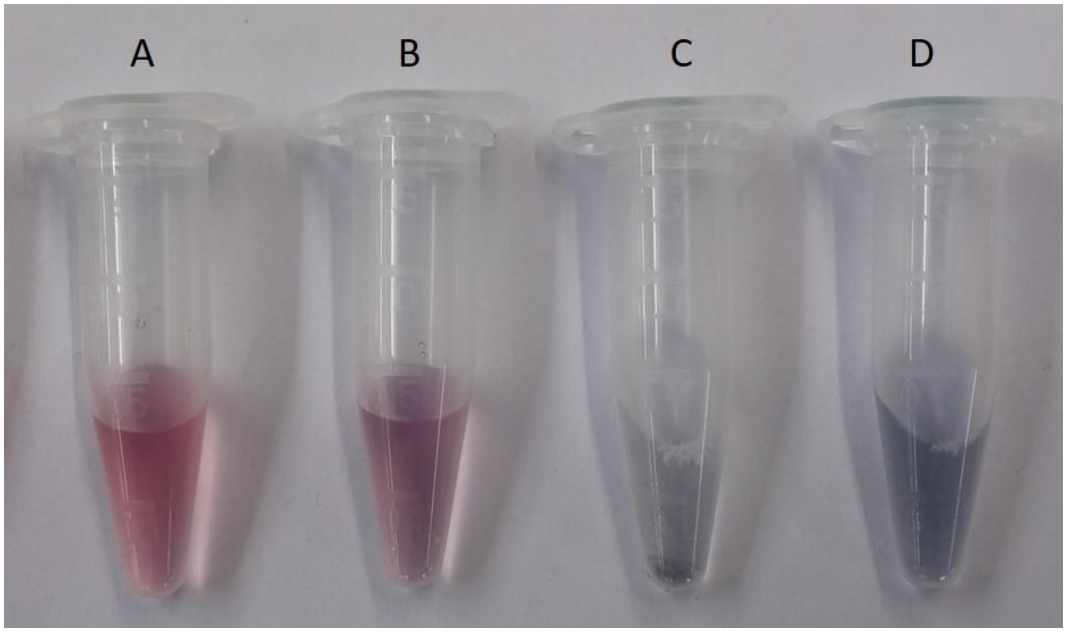


Figure 3.16: Modified AuNP based Telomerase Activity Assay Colour Change. This image shows the colour change of the nanoparticle solution after performing the AuNP assay. (A) contains unmodified AuNPs as well as the reaction buffer necessary for the telomere extension reaction and has a red colour. (B) contains DNA modified AuNPs as well as the reaction buffer and has a light purple colour. (C) contains the DNA modified AuNPs, reaction buffer and protein extract, where aggregation can easily be seen at the bottom of the tube. (D) contains the same components as C, however the extension reaction has been allowed to proceed. This Sample has a light blue colour and very little aggregation is present.

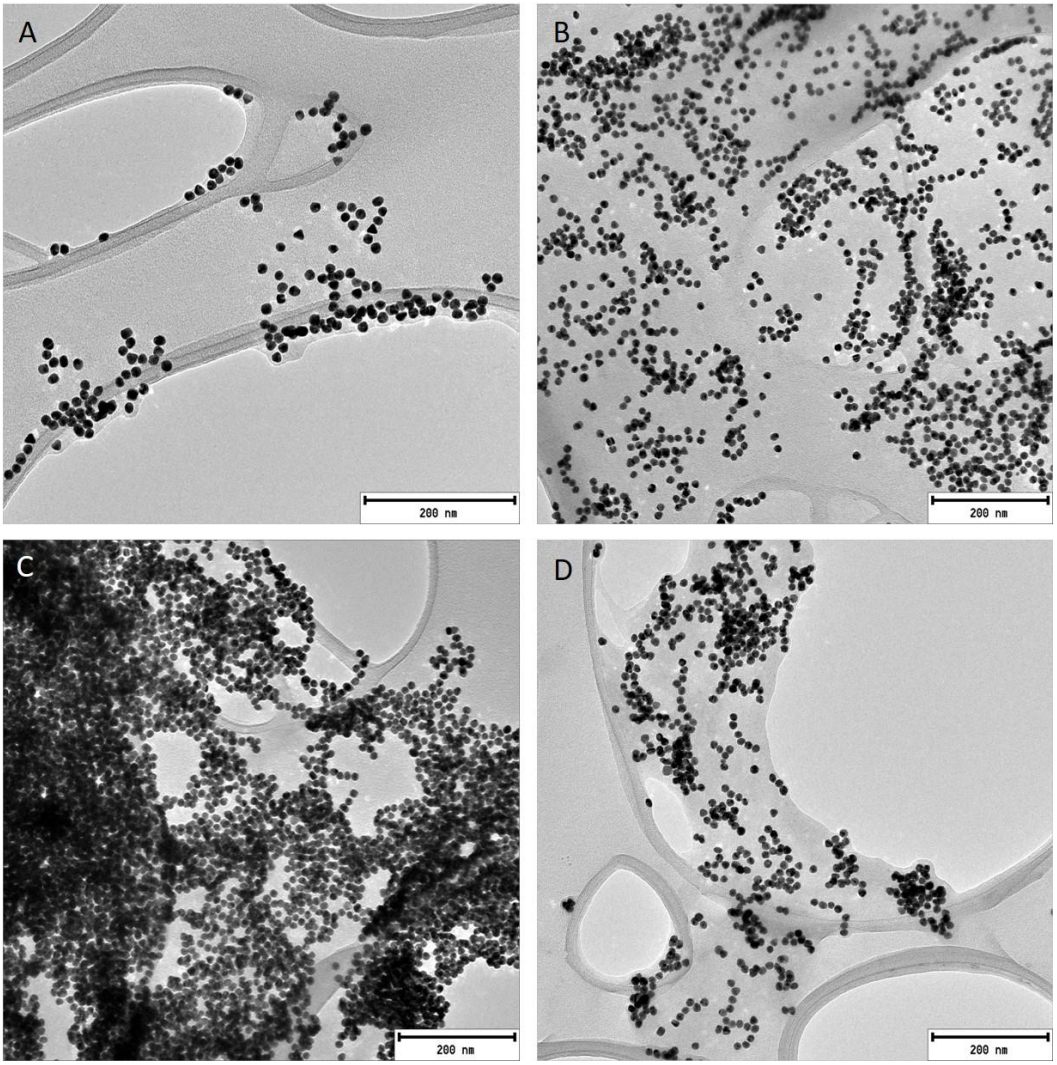


Figure 3.17: Transmission Electron Microscopy Analysis of the Modified AuNP Based Telomerase Activity Assay. This image shows unmodified AuNPs (A), which are largely dispersed. The DNA functionalised AuNPs (B) show increased association with one another. (C) shows DNA modified AuNPs in the presence of a protein extract. Here high amounts of aggregation can be seen. (D) on the other hand, shows the same sample as seen in C, however the telomere extension reaction was performed. This sample still shows signs of aggregation, but far less that that seen in (C).

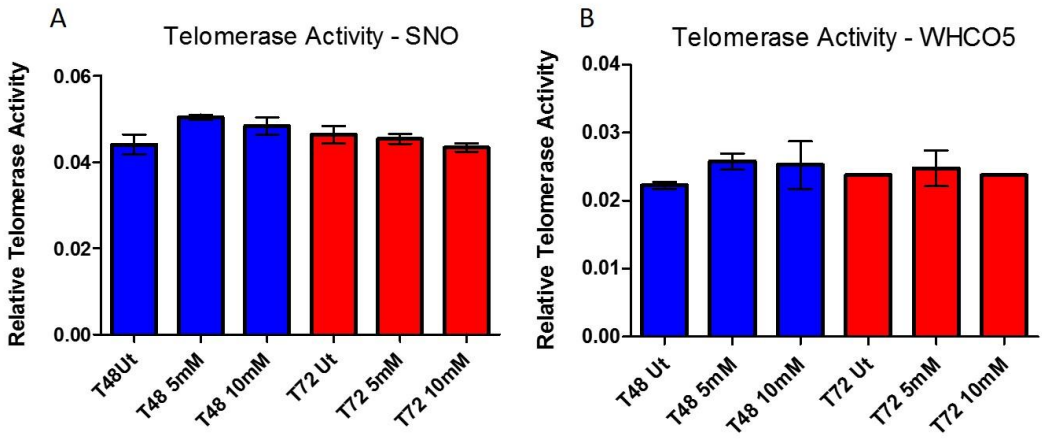


Figure 3.18: Relative Telomerase Activity of the AuNP Based Telomerase Activity Assay in SNO and WHCO5 Cells. After the telomere extension reaction, the absorbance of the nanoparticle solutions containing protein extracts from metformin treated SNO (A) and WHCO5 (B) cell lines was obtained. No significant difference could be seen between treated and untreated samples within the cell lines.

# 4 Discussion:

## 4.1 Cell Viability:

In this study, metformin was found to affect telomere dynamics. It was clear that cells cultured in the presence of the drug had higher amounts of detachment compared to that of the untreated controls. This was assumed to be the cause of decreased cell viability due to the treatment. After performing MTT cell viability assays however, it was found that HEK293, MRC5, SNO and WHCO1 cell lines did not have a significant decrease in cell viability (Figure 3.1). This would suggest that the detachment is not necessarily a sign of cell death, but may be due to metformin interfering with cell-surface adhesion proteins such as Integrin-linked Kinase (ILK) (Vespa et al., 2005). In fact, it has been shown that metformin can decrease ILK gene expression through the indirect regulation of Sp1 and AP-2α (Activating Protein 2 α) protein expressions (Hahn et al., 2014). The number of viable cells could be determined using a trypan blue assay on the detached cells to determine if this is indeed the case. The WHCO5 cell line did show a significant decrease in cell viability in both the 48 and 72 h treatments whereas the WHCO1 cell line did not (Figure 3.1). The reason for this is currently unknown and would require further research. Since both WHCO1 and WHCO5 cell lines possess wild type p53 (Fanucchi and Veale, 2009), it could be possible that due to a mutation, metformin is unable to activate the p53 tumour suppressor within the WHCO1 cell line.

## 4.2 Metformin Decreases Telomere Length:

Telomere length has been associated with cell viability (Sahin and Depinho, 2010) and is therefore an important factor to consider after treatment. Metformin was also shown to significantly decrease telomere length in the WHCO5 cell line after 48 h but not after 72 h, although a downward trend was visible in the 5 mM 72 h treatment. Whereas the SNO cell line showed a significant decrease in telomere length after 72 h (Figure 3.2). This was unexpected, as the treatment was only

performed for up to 72 h and should therefore not have resulted in significantly reduced telomere length. An alternate explanation may be that the results are due to the increased stress of the treatment, resulting in a loss of telomere integrity. The literature has shown that metformin indeed increases oxidative stress in neuroblastoma cells (Picone et al., 2015) and white adipocytes (Anedda et al., 2008). A decrease in telomere length due to oxidative stress has also previously been reported due to a variety of factors, including lifestyle variables such as smoking (Babizhayev et al., 2011) and lifestyle diseases such as type 2 diabetes (Sampson et al., 2006).

### 4.3 Metformin Reduces Telomerase Activity:

Metformin significantly decreased telomerase activity in HEK293, WHCO5 and SNO cells, and caused a downward trend in the WHCO1 cell line (Figure 3.4). The MRC5 cell line had very low/ undetectable levels of telomerase activity, which is consistent with the literature, as normal somatic cell lines generally express low amounts of telomerase (Kim et al., 1994). This coupled with the fact that metformin does not influence telomerase at the DNA level (Bernert, 2014) and that hTERT mRNA expression was not influenced by the metformin treatment in the WHCO5 cell line (Figure 3.3), which is in contrast to previous findings in the literature where metformin decreased hTERT mRNA expression in endometrial cancer (Hanna et al., 2012), seems to suggest that metformin may acts on the protein level in oesophageal cancer. It is however not known if it is a direct association to hTERT or the telomerase enzyme as a whole. Despite this, metformin significantly decreased telomerase activity and may therefore be a suitable treatment option, in conjunction with conventional therapies, to treat oesophageal cancer and perhaps other cancers that utilise increased telomerase activity to bypass senescence.

## 4.4 Successful Nanoparticle Synthesis:

Silver, platinum and gold nanoparticles were successfully synthesised using chemical hydrothermal metal salt reduction. Absorbance spectra and SEM and TEM images of all samples were taken to determine size distribution of the particles. The spectrophotogram of the silver nanoparticles (Figure 3.5) showed a wide peak, which suggested that the synthesised nanoparticles had a large size range. This was later confirmed by the electron microscopy of the brown nanoparticle solution, where the TEM image (Figure 3.6 B) showed the presence of nano-triangles, nano-rods and spherical nanoparticles. The spectrophotogram of the platinum nanoparticles (Figure 3.7) on the other hand had no discernible peak, which made it impossible to determine the size distribution and it was thought that the synthesis had failed. The colour of the solution did change to a dark yellow however and the SEM and TEM images (Figure 3.8) confirmed platinum nanoparticle synthesis, however the particles were difficult to distinguish. This spectrophotogram is however consistent with the literature for platinum nanoparticles. The gold nanoparticles were very easily synthesised, and their sizes were easily controlled. The solutions also had very clear colour changes as the nanoparticles increased in size (Figure 3.9). The spectrophotogram of the gold nanoparticles (Figure 3.10) showed a relatively slim peak, which is consistent with uniform nanoparticle size. This was confirmed using TEM (Figure 3.11 B), where the nanoparticles had a very uniform morphology. Mostly nano-spheres were found, with very few nano-triangles and no nano-rods present. After an ImageJ analysis, it was found that the average size of the particles was 13 nm.

## 4.5 Successful Protein Functionalisation of Platinum Nanoparticles:

Before coupling the nanoparticles to the synthetic telomeric DNA, a proof-of-concept experiment was performed to show that the colour of the nanoparticle solution would change due to the presence of attached molecules. Platinum nanoparticles were functionalised with lysozyme, as it was thought that the platinum would more easily associate with the amide groups present in the protein.

There was no visible colour change after the protein functionalisation, however TEM images did show coat was present on the nanoparticles compared to the control (Figure 3.12 B). This coat may be the protein associating with the nanoparticles, unfortunately the platinum nanoparticles were difficult to distinguish under TEM. Due to this, as well as the difficulty in seeing a colour change, gold nanoparticles were used for the DNA functionalisation experiments.

## 4.6 Successful DNA Functionalisation of AuNPs:

Due to the success of the previous protein functionalisation experiment, DNA functionalisation was performed. For the DNA functionalisation experiments, the small 13 nm diameter red AuNP solution was used, as the colour of the solution would shift towards blue if the particles would move further apart from one another. After functionalisation, the colour of the solution visibly turned to a more purple colour and the spectrophotogram showed both a shift in the peak as well as the presence of the DNA at 260 nm (Figure 3.13). This seemed to show that the AuNPs were either acting as larger nanoparticles due to the presence of the DNA on their surface or that they were more closely associated. This close association could however be due to the DNA on the particles directly binding to one another (Hill et al., 2009). It was confirmed, using TEM (Figure 3.14), that a distinct halo was present surrounding the DNA coupled AuNPs but not the untreated control, which seems to indicate that the nanoparticles do indeed act as larger particles when functionalised. Light scattering was then performed on the samples using a Zetasizer to determine any change in the relative size of the nanoparticles (Figure 3.15). The 13 nm diameter AuNPs (determined using TEM) gave a reading of 40 nm. This is due to the Zetasizer measuring the hydrodynamic size of the particles, where it takes the surrounding liquid molecules into consideration. This measurement is often larger than the actual size of the particle. The DNA functionalised sample showed a second peak at 110 nm. This suggests that not all the nanoparticles were functionalised and those that were showed an increased hydrodynamic size. A third solution was measured, containing functionalised nanoparticles as well as protein extract, to determine the effects of the proteins on

the size of the functionalised nanoparticles. This third sample showed both the 40 nm and 110 nm peaks as well as a very broad peak towards the micron size range, indicating aggregation. Light scattering showed that there was a definite change in the diameter of the nanoparticles after the addition of the thiolated DNA, confirming DNA functionalisation.

## 4.7 AuNP Based Telomerase Activity Assay:

After successful DNA functionalisation, the AuNP based telomerase activity assay was performed. As the extracted telomerase, in the protein extract, elongated the synthetic telomeres. It was thought that the nanoparticles would act as larger AuNPs due to the increased diameter of the nanoparticles and the elongated DNA and therefore cause a blue shift in the colour of the solution. There was a distinct colour change from the purple of the DNA-functionalised AuNP solution (Figure 3.16 B) to a light blue after the addition of the protein extract (Figure 3.16 C). This was then followed by aggregation. In the sample where the attached DNA was elongated however, there was significantly less aggregation and the dark blue colour was easily visible (Figure 3.16 D). This would suggest that the elongated DNA serves not only to increase the distance between particles, thereby treating them as larger particles, and causing a colour shift, but also to resist aggregation of the particles. This resistance to aggregation should then be measurable by spectrophotometry. This resistance to aggregation was then confirmed using TEM (Figure 3.17). The unmodified AuNPs were very dispersed (Figure 3.17 A), and only slightly more association between particles in the DNA modified AuNP sample was observed (Figure 3.17 B). The sample containing both DNA functionalised AuNPs and protein extract, predictably showed massive aggregation (Figure 3.17 C). The sample where the DNA was elongated by telomerase (Figure 3.17 D) showed significantly less aggregation than the non-elongated sample (Figure 3.17 C). For the metformin treatments, SNO and WHCO5 protein extracts were then used to elongate the telomeric substrate using a short PCR step. Absorbance readings were then taken of the resulting nanoparticle solutions (Figure 3.18). Unfortunately, both the SNO and WHCO5 cell lines showed no significant difference between the

untreated and treated samples. This contrasts with the telomerase activity data obtained using qPCR, where both cell lines exhibited a decrease in telomerase activity. Although a difference was seen between non-elongated samples and elongated samples, the assay was not sensitive enough to differentiate between treated and untreated samples of the same cell line. This may be partially due to the presence of unmodified AuNPs, as seen by the light scattering results, causing additional aggregation. However, since TEM images confirmed a difference in aggregation despite the presence of unmodified AuNPs, the lack of significant results is likely due to the measurement technique not being sensitive enough.

## 4.8 Conclusion:

In conclusion, the MTT assay showed that only the WHCO5 cell line had a significant decrease in cell viability despite large amounts of cell detachment in the other cell lines. Cell detachment may therefore not be an indicator of cell viability after metformin treatment. Metformin also affected telomere length but not hTERT mRNA expression, which is in contrast to previous findings where metformin decreased hTERT mRNA expression in endometrial cancer (Hanna et al., 2012). Metformin significantly reduced telomeres activity in HEK293, SNO, WHCO5 cell lines and caused a downward trend in the WHCO1 cell line. This could therefore potentially be used in conjunction with conventional anti-cancer treatments for a more effective method of treating cancers that use increased telomerase activity to bypass senescence. AuNPs were successfully synthesised and functionalised with thiolated DNA (telomerase substrate). The nanoparticles were then characterised and visualised using spectrophotometry and electron microscopy. The AuNP based telomerase activity assay was then performed on the SNO and WHCO5 cell lines, but treated samples did not show any significant difference to the untreated samples. This assay does however have great potential in becoming a cheaper, faster alternative to that of the conventional qPCR based techniques once further optimised.

## 4.9 Future Work:

Future work will include an alternative to the MTT cell viability assay, possibly the alamarBlue assay, to confirm the results obtained. Trypan blue assays will also be performed on detached cells to determine if the cells are indeed dead or simply detaching due to the metformin treatment. Western blots will also be performed to determine the total hTERT protein levels in the cell lines. Protein association studies can also be done to determine if metformin directly binds to hTERT, hTERC or the larger telomerase enzyme. The AuNP telomerase activity assay can also be improved by optimising the DNA functionalisation step further to reduce the number of non-functionalised nanoparticles within the solution. It would also be beneficial to scale up the AuNP experiment (from 50 µl to 300 µl), to have a larger volume of sample to test. This would make it possible to test one sample using multiple techniques such as light scattering and UV-spectroscopy, which are more sensitive than absorption spectrophotometry.

## 5 References:


Anedda, A., Rial, E., and González-Barroso, M.M. (2008). Metformin induces oxidative stress in white adipocytes and raises uncoupling protein 2 levels. Journal of Endocrinology. *199*, 33–40.

Arnold, M., Soerjomataram, I., Ferlay, J., and Forman, D. (2015). Global incidence of oesophageal cancer by histological subtype in 2012. Gut *64*, 381–387.

Babizhayev, M.A., Savel'yeva, E.L., Moskvina, S.N., and Yegorov, Y.E. (2011). Telomere Length is a Biomarker of Cumulative Oxidative Stress, Biologic Age, and an Independent Predictor of Survival and Therapeutic Treatment Requirement Associated With Smoking Behavior. American Journal of Therapeutics. *18*, 209–226.

Bailey, S.M., and Murnane, J.P. (2006). Telomeres, chromosome instability and cancer. Nucleic Acids Research. *34*, 2408–2417.

Baird, D.M., Rowson, J., Wynford-Thomas, D., and Kipling, D. (2003). Extensive allelic variation and ultrashort telomeres in senescent human cells. Nature Genetics. *33*, 203–207.

Bernert, M. (2014). Metformin reduces telomerase activity in oesophageal carcinoma cells expressing wild-type p53. BSc Honours Dissertation. University of the Witwatersrand.

Bey, E., Alexander, J., Whitcutt, J.M., Hunt, J.A., and Gear, J.H.S. (1976). Carcinoma of the esophagus in africans: Establishment of a continuously growing cell line from a tumor specimen. In Vitro *12*, 107–114.

Blackburn, E.H. (1991). Structure and function of telomeres. Nature *350*, 569–573.

Britt-Compton, B., Rowson, J., Locke, M., Mackenzie, I., Kipling, D., and Baird, D.M. (2006). Structural stability and chromosome-specific telomere length is

governed by cis-acting determinants in humans. Human Molecular Genetics *15*, 725–733.

Brown, L.M., Hoover, R., Silverman, D., Baris, D., Hayes, R., Swanson, G.M., Schoenberg, J., Greenberg, R., Liff, J., Schwartz, A. (2001). Excess Incidence of Squamous Cell Esophageal Cancer among US Black Men: Role of Social Class and Other Risk Factors. American Journal of Epidemiology. *153*, 114–122.

Bryan, T.M., and Reddel, R.R. (1997). Telomere dynamics and telomerase activity in in vitro immortalised human cells. European Journal of Cancer. *33*, 767–773.

Buzzai, M., Jones, R.G., Amaravadi, R.K., Lum, J.J., DeBerardinis, R.J., Zhao, F., Viollet, B., and Thompson, C.B. (2007). Systemic treatment with the antidiabetic drug metformin selectively impairs p53-deficient tumor cell growth. Cancer Research. *67*, 6745–6752.

Capper, R., Britt-compton, B., Tankimanova, M., Rowson, J., Letsolo, B., Man, S., Haughton, M., and Baird, D.M. (2007). The nature of telomere fusion and a definition of the critical telomere length in human cells. Genes & Development. *21*, 2495–2508.

Carlin, A.S., Grant, I., Adams, K.M., Reed, R., Am, J., Nakamura, T.M., Morin, G.B., Chapman, K.B., Weinrich, S.L., Andrews, W.H. (1997). Telomerase Catalytic Subunit Homologs from Fission Yeast and Human. Science. *277*, 955–960.

Carneiro, M.C., Henriques, C.M., Nabais, J., Ferreira, T., Carvalho, T., Ferreira, M.G. (2016). Short Telomeres in Key Tissues Initiate Local and Systemic Aging in Zebrafish. PLoS Genetics. 12(1), e1005798.

Choong-kun, L., Minkyu, J., Inkyung, J., Su Jin, H., Yong Hyu, J., Ji Yeong, A., Hyoung-Il, K., Jae-Ho, C., Woo Jin, H., Sung Hoon, N., Hyo Song, K., Sun Young, R., Hyun Cheol, C. (2016). Cumulative Metformin Use and Its Impact on Survival in Gastric Cancer Patients After Gastrectomy. Annals of Surgery. 263 (1), 96–102.

Damelin, L.H., Jivan, R., Veale, R.B., Rousseau, A.L., Mavri-Damelin, D. (2014). Metformin induces an intracellular reductive state that protects oesophageal squamous cell carcinoma cells against cisplatin but not copper-bis(thiosemicarbazones). BMC Cancer. *14*, 314–325.

Denchi, E.L. (2009). Give me a break: how telomeres suppress the DNA damage response. DNA Repair. *8*, 1118–1126.

Domper Arnal, M. J., Ferrández Arenas, Á., & Lanas Arbeloa, Á. (2015). Esophageal cancer: Risk factors, screening and endoscopic treatment in Western and Eastern countries. World Journal of Gastroenterology. 21(26), 7933–7943.

Fanucchi, S., and Veale, R.B. (2009). Role of p53/FAK association and p53Ser46 phosphorylation in staurosporine-mediated apoptosis: wild type versus mutant p53-R175H. FEBS Letters.*583*, 3557–3562.

Graham, F.L., Smiley, J., Russell, W.C., and Nairn, R. (1977). Characteristics of a human cell line transformed by DNA from human adenovirus type 5. J. Journal of General Virology. *36*, 59–74.

Greenberg, R., O'Hagan, R.C., Deng, H., Xiao, Q., Hann, S.R., Adams, R.R., Lichtsteiner, S., Chin, L., Morin, G.B., and DePinho, R. (1999). Telomerase reverse transcriptase gene is a direct target of c-Myc but is not functionally equivalent in cellular transformation. Oncogene. *18*, 1219–1226.

Haendeler, J., Dröse, S., Büchner, N., Jakob, S., Altschmied, J., Goy, C., Spyridopoulos, I., Zeiher, A.M., Brandt, U., Dimmeler, S. (2009). Mitochondrial telomerase reverse transcriptase binds to and protects mitochondrial DNA and function from damage. Arteriosclerosis, Thrombosis, and Vascular Biology. *29*, 929–935.

Hahn, Sw.S., Tang, Q., Zheng, F., Zhao, S., Wu, J., and Chen, J. (2014). Repression of integrin-linked kinase by antidiabetes drugs through cross-talk of PPARγ- and AMPKα-dependent signaling: Role of AP-2α and Sp1. Cellular Signalling. *26*, 639–647.

Hanna, R.K., Zhou, C., Malloy, K.M., Sun, L., Zhong, Y., Gehrig, P. a, and Bae-Jump, V.L. (2012). Metformin potentiates the effects of paclitaxel in endometrial cancer cells through inhibition of cell proliferation and modulation of the mTOR pathway. Gynecologic Oncology. *125*, 458–469.

Harris, S.E., Martin-Ruiz, C., von Zglinicki, T., Starr, J.M., and Deary, I.J. (2012). Telomere length and aging biomarkers in 70-year-olds: The Lothian Birth Cohort 1936. Neurobiology of Aging. *33*, 1486–1491.

Hayflick, L., and Moorhead, P.S. (1961). The Serial Cultivation of Human Diploid Cell Strains. Experimental Cell Research. *25*, 585–621.

Hill, H.D., Hurst, S.J., and Mirkin, C.A. (2009). Curvature-Induced Base Pair "Slipping" Effects in DNA- Nanoparticle Hybridization. Nano Letters. *9*, 317–321.

Hirsch, H.A., Iliopoulos, D., Tsichlis, P.N., Struhl, K. (2009). Metformin selectively targets cancer stem cells, and acts together with chemotherapy to block tumor growth and prolong remission. Cancer Research. *69*, 7507–7511.

Hofer, P., Zerelles, J., Baierl, A., Madersbacher, S., Schatzl, G., Maj-Hes, A., Sutterlüty-fall, H., Gsur, A. (2013). MNS16A tandem repeat minisatellite of human telomerase gene and prostate cancer susceptibility. Mutagenesis. *28*, 301–306.

Jacobs, J.P., Jones, C.M., and Baille, J.P. (1970). Characteristics of a Human Diploid Cell Designated MRC-5. Nature. *227*, 168–170.

Jemal, A., Bray, F., Center, M.M., Ferlay, J., Ward, E., and Forman, D. (2011). Global cancer statistics. CA: A Cancer Journal for Clinicians. *61*, 69–90.

Josie M.M. Evans, Louise A Donnelly, Alistair M Emslie-Smith, Dario R Alessi, A.D.M. (2005). Metformin and reduced risk of cancer in diabetic patients. BMJ *330*, 1304–1305.

Kanaya, T., Kyo, S., Hamada, K., Takakura, M., Kitagawa, Y., Harada, H., Inoue, M. (2000). Adenoviral expression of p53 represses telomerase activity through

down-regulation of human telomerase reverse transcriptase transcription. Clinical Cancer Research. *6*, 1239–1247.

Kim, N.W., Piatyszek, M.A., Prowse, K.R., Harley, C.B., West, D., Ho, P.L.C., Coviello, G.M., Wright, W.E., Weinrich, S.L., Shay, W., et al. (1994). Specific Association of Human Telomerase Activity with Immortal Cells and Cancer. Science. *266*, 2011–2015.

Kirkpatrick, K.L., Clark, G., Ghilchick, M., Newbold, R.F., and Mokbel, K. (2003). hTERT mRNA expression correlates with telomerase activity in human breast cancer. European Journal of Surgical Oncology. *29*, 321–326.

Kovacic, J.C., Moreno, P., Hachinski, V., Nabel, E.G., Fuster, V. (2011). Cellular senescence, vascular disease, and aging: Part 1 of a 2-part review. Circulation. *123*, 1650–1660.

Lawenda, B.D., Kelly, K.M., Ladas, E.J., Sagar, S.M., Vickers, A., Blumberg, J.B. (2008). Should supplemental antioxidant administration be avoided during chemotherapy and radiation therapy? Journal of the National Cancer Institute. *100*, 773–783.

Levy, M.Z., Allsopp, R.C., Futcher, a B., Greider, C.W., and Harley, C.B. (1992). Telomere end-replication problem and cell aging. Journal of Molecular Biology. *225*, 951–960.

Picone, P., Nuzzo, D., Caruana, L., Messina, E., Barera, A., Vasto, S., and Di Carlo, M. (2015). Metformin increases APP expression and processing via oxidative stress, mitochondrial dysfunction and NF-κB activation: Use of insulin to attenuate metformin's effect. Biochimica et Biophysica Acta. *1853*, 1046–1059.

Pusceddu, I., Farrell, C.-J.L., Di Pierro, A.M., Jani, E., Herrmann, W., Herrmann, M. (2015). The role of telomeres and vitamin D in cellular aging and age-related diseases. Clinical Chemistry and Laboratory Medicine. *11:1661-1678.*

Raffa, G.D., Cenci, G., Ciapponi, L., Gatti, M. (2013). Organization and

Evolution of Drosophila Terminin: Similarities and Differences between Drosophila and Human Telomeres. Frontiers in Oncology. *3*, 112.

Sahin, E., and Depinho, R.A. (2010). Linking functional decline of telomeres, mitochondria and stem cells during ageing. Nature. *464*, 520–528.

Sampson, M.J., Winterbone, M.S., Hughes, J.C., Dozio, N., Hughes, D.A. (2006). Monocyte Telomere Shortening and Oxidative DNA Damage in Type 2 Diabetes. Diabetes Care. *29*, 283–289.

Saretzki, G. (2009). Telomerase, mitochondria and oxidative stress. Experimental Gerontology. *44*, 485–492.

Shay, J.W., and Wright, W.E. (2005). Senescence and immortalization: Role of telomeres and telomerase. Carcinogenesis. *26*, 867–874.

Sheng, X., Tong, N., Tao, G., Luo, D., Wang, M., Fang, Y., Li, J., Xu, M., Zhang, Z., Wu, D. (2013). TERT polymorphisms modify the risk of acute lymphoblastic leukemia in Chinese children. Carcinogenesis. *34*, 228–235.

Tang, B., Xie, R., Qin, Y., Xiao, Y.F., Yong, X., Zheng, L., Dong H., Yang, S.M. (2016). Human telomerase reverse transcriptase (hTERT) promotes gastric cancer invasion through cooperating with c-Myc to upregulate heparanase expression. Oncotarget. 7(10), 11364–11379.

Tran, S.-L., Puhar, A., Ngo-Camus, M., Ramarao, N. (2011). Trypan Blue Dye Enters Viable Cells Incubated with the Pore-Forming Toxin HlyII of Bacillus cereus. PLoS One. *6*, e22876.

Tseng, C.-H. (2016). Metformin may reduce oral cancer risk in patients with type 2 diabetes. Oncotarget. 7(2), 2000–2008.

Veale, R.B., and Thornley, A.L. (1989). Increased Single Class Low-Affinity EGF Receptors Expressed by Human Oesophageal Squamous Carcinoma Cell Lines. South African Journal of Science. *85*, 375–379.

Vespa, A., D ’souza, S.J.A., Dagnino, L. (2005). A Novel Role for Integrin-linked

Kinase in Epithelial Sheet Morphogenesis. Molecular Biology of the Cell. *16*, 4084–4095.

Wang, J., Wu, L., Ren, J., and Qu, X. (2012). Visualizing human telomerase activity with primer-modified Au nanoparticles. Small. *8*, 259–264.

Wang, L., Soria, J.-C., Chang, Y.-S., Lee, H.-Y., Wei, Q., Mao, L. (2003). Association of a functional tandem repeats in the downstream of human telomerase gene and lung cancer. Oncogene. *22*, 7123–7129.

Wright, W.E., Piatyszek, M.A., Rainey, W.E., Byrd, W., Shay, J.W. (1996). Telomerase Activity in Human Germline and Embryonic Tissues and Cells. Developmental Genetics. *18*, 173–179.

Yarbakht, M., and Nikkhah, M. (2016). Unmodified gold nanoparticles as a colorimetric probe for visual methamphetamine detection. Journal of Experimental Nanoscience. *11*, 593–601.

Zakikhani, M., Dowling, R., Fantus, I.G., Sonenberg, N., Pollak, M. (2006). Metformin Is an AMP Kinase–Dependent Growth Inhibitor for Breast Cancer Cells. Cancer Research. *66*, 10269–10273.

Zhang, Y., Toh, L., Lau, P., Wang, X. (2012). Human telomerase reverse transcriptase (hTERT) is a novel target of the Wnt/β-catenin pathway in human cancer. Journal of Biological Chemistry. *287*, 32494–32511.

Zhou, X., and Xing, D. (2012). Assays for human telomerase activity: progress and prospects. Chemical Society Reviews. *41*, 4643–4656.

Zhu, G., Yang, K., Zhang, C. (2015). A single quantum dot-based biosensor for telomerase assay. Chemical Communications. *51*, 6808–6811.

Electronic References:

GLOBOCAN 2012 – Estimated Cancer Incidence, Mortality and Prevalence Worldwide in 2012. (accessed on 15.03.2015). http://globocan.iarc.fr/Pages/fact_sheets_cancer.aspx

Figure 1.5: Telomerase: http://www.canoadetolda.org.br/biolmol/aula2_DNAestrutrep.htm (Accessed on 09.03.2014)

# 6 Appendix:

## 6.1 Materials used:

| Table 1A: Cell Culture Reagents | |
|---|---|
| **Product** | **Supplier** |
| Cell Culture Flasks (75cm) | Sigma Aldrich |
| DMEM | Sigma Aldrich |
| L-Glutamine | Sigma Aldrich |
| Penicillin-Streptomycin | Celtic |
| Foetal Calf Serum | Celtic |
| Trypsin/EDTA | Celtic |
| Metformin | Sigma Aldrich |
| MTT | Sigma Aldrich |

| Table 2A: DNA/RNA Reagents | |
|---|---|
| **Product** | **Supplier** |
| Quick-RNA Mini Prep Kit | Zymo Research |
| ProtoScript First Strand cDNA synthesis Kit | New England BioLabs |
| Tris | Signa Aldrich |
| Glycerol | Signa Aldrich |
| SDS | Signa Aldrich |
| Mercaptoethanol | Signa Aldrich |
| Proteinase K | Inqaba Biotech |
| Ethanol | Signa Aldrich |
| Isopropanol | Signa Aldrich |
| Phenol–chloroform | Signa Aldrich |

| Table 3A: PCR/qPCR Reagents and Primers | |
|---|---|
| **Product** | **Supplier** |
| MNS16A Primers | Inqaba Biotech |
| GAPDH Primers | Inqaba Biotech |
| KAPA Taq | Lasec |
| GRGreen | Inqaba Biotech |
| EvaGreen | GeneDireX |
| SeaKem® LE Agarose | Lonza |
| (10x) TBE Buffer | Sigma Aldrich |

| | |
|---|---|
| (10x) TAE Buffer | Sigma Aldrich |
| 1kb DNA Ladder | Separations |
| TRAPeze RT Telomerase Detection Kit | Merck-Millipore |

| **Table 4A: STELA Reagents and Primers** | |
|---|---|
| **Product** | **Supplier** |
| TeloTAGGG kit | UTI Pharma |
| Nitrocellulose Membrane | Separations |
| Primer: 17pseq1rev | Inqaba Biotech |
| Primer: XpYpE | Inqaba Biotech |
| Primer: Teltail | Inqaba Biotech |
| Primer: Telorette2 | Inqaba Biotech |

| **Table 5A: AuNP Synthesis/Functionalisation** | |
|---|---|
| **Product** | **Supplier** |
| Chloroauric acid | Sigma Aldrich |
| Citric acid | Sigma Aldrich |
| Thiolated Oligonucleotides (Telomerase Substrate) | Inqaba Biotech |

6.2 Buffer Compositions:

Table 6A: DNA Extraction Buffer:

| **Compound** | **Final Percentage** |
|---|---|
| Tris-HCL (pH 6.8) | 45 % (0.2 M) |
| Glycerol | 45 % |
| SDS | 5 % |
| Mercaptoethanol | 5 % |

Table 7A: Nanoparticle Assay Telomere Elongation Buffer:

| **Compound** | **Final Concentration** |
|---|---|
| Tris-HCL (pH 8.3) | 20 mM |
| KCl | 6.3 mM |
| EGTA | 1 mM |
| Tween-20 | 0.005 % |
| BSA | 0.1 mM |
| MgCL | 1.5 mM |
| dNTPs | 1 mM |

Table 8A: Cell Culture Medium:

| Compound | Percentage |
|---|---|
| Dulbecco's Modified Eagle's Medium | 88 % |
| Foetal Calf Serum | 10 % |
| Penicillin-Streptomycin | 1 % |
| L-Glutamine | 1 % |

6.3 Equipment Used:

Table 9A: Equipment Used:

| Equipment | Manufacturer |
|---|---|
| Neubauer haemocytometer | Sigma Aldrich |
| 1-14 Microcentrifuge | Sigma Aldrich |
| ND1000 NanoDrop spectrophotometer | Thermo Scientific |
| MJ Mini thermal cycler | BioRad |
| ChemiDoc | BioRad |
| LightCycler 480 (qPCR) | Roche |
| UV-1800 Spectrophotometer | Shimadzu |
| FEI Quanta FEG-SEM | Fei |
| FEI Spirit 120 kV TEM | Fei |
| Zetasizer | Malvern |